An arms race between 5'ppp-RNA virus and its alternative recognition receptor MDA5 in RIG-I-lost teleost fish

Shang Geng[1], Xing Lv[1], Weiwei Zheng[1], Tianjun Xu[1,2,3,*]

1. *Laboratory of Fish Molecular Immunology, College of Fisheries and Life Science, Shanghai Ocean University, Shanghai, China*
2. *Laboratory for Marine Biology and Biotechnology, Qingdao Marine Science and Technology Center, Qingdao, China*
3. *Marine Biomedical Science and Technology Innovation Platform of Lin-gang Special Area, Shanghai, China*

*Corresponding author. Dr. Tianjun Xu

E-mail: tianjunxu@163.com

Running title: MDA5 recognizes 5'ppp-RNA virus in species lacking RIG-I

Abstract: The incessant arms race between viruses and hosts has led to numerous evolutionary innovations that shape life's evolution. During this process, the interactions between viral receptors and viruses have garnered significant interest since viral receptors are cell surface proteins exploited by viruses to initiate infection. Our study sheds light on the arms race between the MDA5 receptor and 5'ppp-RNA virus in a lower vertebrate fish, *M. miiuy*. Firstly, the frequent and independent loss events of RIG-I in vertebrates prompted us to search for alternative immune substitutes, with homology-dependent genetic compensation response (HDGCR) being the main pathway. Our further analysis suggested that MDA5 of *M. miiuy and G. gallus*, the homolog of RIG-I, can replace RIG-I in recognizing 5'ppp-RNA virus, which may lead to redundancy of RIG-I and loss from the species genome during evolution. Secondly, as an adversarial strategy, 5'ppp-RNA SCRV can utilize the m^6A methylation mechanism to degrade MDA5 and weaken its antiviral immune ability, thus promoting its own replication and immune evasion. In summary, our study provides a snapshot into the interaction and coevolution between vertebrate and virus, offering valuable perspectives on the ecological and evolutionary factors that contribute to the diversity of the immune system.

Keywords: RIG-I; MDA5; 5'ppp-RNA; Genetic compensation response; Pattern recognition receptors; Immune evasion

1. Introduction

The Pattern recognition receptors (PRRs) recognize conserved pathogen-associated molecular pattern (PAMP) motifs, including proteins, lipids and nucleotides, resulting in activation of innate immune responses of host[1]. Retinoic acid-induced RIG-I-like receptors (RLRs) are a specific group of PRRs belonging to the family of DExD/H-box RNA helicases, and they play a crucial role in the innate antiviral response. There are three members in the RLR family: retinoic acid-inducible gene I (RIG-I), melanoma differentiation-associated gene 5 (MDA5), and laboratory of genetics and physiology 2 (LGP2). RIG-I and MDA5 exhibit similar signaling characteristics and structural homology, including two N-terminal caspase-recruitment domains (CARDs), a DExD/H box RNA helicase domain, and a C-terminal repressor domain (RD)[2]. However, LGP2 lacks CARD domain[2]. The specific roles of RIG-I and MDA5 in response to virus stimulation are not redundant: RIG-I detects short blunt-end RNA with a 5'-triphosphate motif (5’ppp-RNA), while MDA5 specifically recognizes long forms of viral dsRNA[3-5]. In contrast, the involvement of LGP2 in cytosolic RNA sensing remains a topic of debate. Some studies have proposed that LGP2 is crucial for the production of type I interferon (IFN-I) in response to several RIG-I- and MDA5-dependent viruses[6], whereas others have described LGP2 as a negative regulator of RIG-I signaling[7]. However, surprisingly, despite the important immune functions of RLR members, they have been lost from the genome in many species including mammals, birds, and fish[8-10].

5’ppp-RNA is present in a wide variety of RNA viruses, including Flaviviridae, Paramyxoviridae, Coronaviridae, Orthomyxoviridae, and Rhabdoviridae families[4]. These viruses widely infect all kinds of life and cause various harmfulness and serious diseases, and the infected

63 hosts range from the highest vertebrates to the lowest vertebrate, teleost fish [11, 12]. 5'ppp-RNA
64 viruses are expected to be recognized and trigger an antiviral immune response by RIG-I.
65 However, RIG-I is lacking in many vertebrates, so who then recognizes 5'ppp-RNA in these
66 species? When a gene is functionally inactive or lost, other genes or pathways may undergo
67 homology-dependent genetic compensation response (HDGCR) to maintain organismal balance.
68 The pressure from viral infections has led to the evolution of the immune system, and the loss of
69 RIG-I may be accompanied by functional substitution by homologous genes in order to
70 compensate for the loss of RIG-I function. *Tupaia belangeri*, a mammal lacking RIG-I, has been
71 reported to possess the MDA5 protein, which has undergone positive selection and exhibits the
72 ability to sense Sendai virus (an RNA virus posed as a RIG-I agonist) for inducing type I IFN[8].
73 This study provides insights into the compensatory mechanism of RIG-I deficiency in vertebrates,
74 however, considering the dynamic nature of host-virus dynamics, further research is urgently
75 needed to validate and expand these insights.

76 For millions of years, viruses have coevolved with their hosts, leading to the development of
77 various mechanisms for immune evasion in response to the mutual evolutionary pressure[13].
78 Recently, it is reported that N6-methyladenosine (m^6A) modification plays a crucial role in
79 enabling viruses to evade the interferon (IFN) response[14]. m^6A methylation is an important
80 epigenetic modification that involves the dynamic and reversible process of RNA methylation,
81 regulated by methylase (writer), demethylase (eraser), and reader proteins that recognize m^6A-
82 modified RNA[15]. N6-methylation deposition on mRNA primarily relies on the enzymatic
83 "writing" complex within the cell, with a key composition featuring methyltransferase-like 3
84 (METTL3) and METTL14. Conversely, N6-demethylation is chiefly modulated by "eraser"

proteins, with fat mass and obesity-associated protein (FTO) and AlkB homolog 5 (ALKBH5) being the identified enzymes for this role [16,17]. The functional impact of N6-methylation on RNA characteristics typically remains latent until recognition by "reader" proteins, such as members of the YTHDF protein family, encompassing YTH domain family 1 (YTHDF1), YTHDF2, and YTHDF3. In mammals, YTHDF2 and YTHDF3 are recognized for their involvement in the degradation of m^6A-modified RNA targets, as well as their association with mRNA localization and phase separation [18]. By utilizing these m^6A-related enzymes in the host, viruses can not only use m^6A modification to hide themselves and avoid recognition by host receptors but also manipulate host gene expression to enable immune evasion [19-21].

Fish and birds are commonly observed to exhibit "RIG-I deficiency" phenomena, and they are also the most abundant groups of aquatic and terrestrial vertebrates respectively, giving them certain evolutionary advantages. As a result, the research of the immune evolution of them helps us to understand the immune evolution of the entire vertebrates. Meanwhile, fish and birds are major source of high-quality protein for human consumption, viral diseases in aquaculture and livestock industry pose serious obstacles to the industry's healthy development. Among them, the 5’ppp-RNA virus, as mentioned earlier, is a highly pathogenic group. Within this group, *siniperca cheats* rhabdovirus (SCRV) is an important pathogen that can cause huge economic losses and serious threats to aquaculture in freshwater and marine fish [22]. In addition, vesicular stomatitis virus (VSV) is also a highly infectious and widely prevalent 5’ppp-RNA virus [12]. Therefore, in this study, we selected teleost fish miiuy croaker (*Miichthys miiuy*) and bird chicken (*Gallus gallus*), two vertebrates lacking RIG-I, as well as two 5'ppp-RNA viruses (SCRV and VSV), to investigate the evolutionary strategies and interactions between 5’ppp-RNA virus and host. The

final results demonstrated that the MDA5 of *M. miiuy* and *G. gallus* lacking RIG-I both evolved the ability to recognize 5'ppp-RNA. In addition, SCRV virus can in turn utilize the m^6A strategy to degrade MDA5 of *M. miiuy* for immune evasion. In summary, these findings shed light on the functional diversity of innate antiviral activity and unveil a complex arms race between virus replication and the innate immunity of its reservoir hosts in vertebrates. In addition, since the loss of RIG-I in vertebrates is a widespread event, our research also provides a new perspective for vertebrate groups that have lost RIG-I.

2. Results

2.1 A genetic compensation response model for RIG loss

In previous studies, it has been reported that a few vertebrates lost the RIG-I gene during evolution [9, 10, 23]. To investigate this further, we analyzed the genomes of various species, and determined the presence and absence of the RIG-I gene. As depicted in Figure 1A, the absence of the RIG-I gene does not appear to be uncommon in vertebrates, with at least three independent loss events observed in mammals, birds and fish, respectively. These gene-loss events occurred over a long evolutionary timescale. Based on the minimum age of the common ancestor of RIG-I-missing species (http://www.timetree.org/), the oldest recorded losses occurring in species like *Erpetoichthys calabaricus*, can be traced back to approximately 330 million years ago (MYA). Conversely, the detected loss in *Gallus gallus* took place less than 42 MYA. To gain a deeper understanding of the evolutionary dynamics of vertebrate RIG-I, we explored the conservation of the genes surrounding RIG-I. We analyzed the genome sequences of *Homo sapiens*, *Callorhinchus milii*, *Danio rerio*, *Tupaia belangeri*, *Gallus gallus*, and *M. miiuy* (Figure 1B). Similar to the slow-evolving *Callorhinchus milii*, humans possess RIG-I with TOPORS and ACO1 as its upstream and downstream genes, respectively. As previously reported[8, 10]. *Tupaia belangeri*, *Gallus gallus*, and *M. miiuy* do not have RIG-I. Interestingly, zebrafish has a RIG-I with its upstream gene being TOPORSb, seemingly a result of chromosome fragment duplication. However, one RIG-I gene was lost in the downstream region of TOPORSa, indicating that one of the RIG-I copies has been lost in zebrafish, similar to *M. miiuy*.

Given the important role of RIG-I in recognizing 5'ppp RNA, we selected two different models for experiments to detect the presence of other potential receptors for immune

137 compensation in RIG-I deficient species. Specifically, we extracted virus RNA from SCRV and
138 VSV viruses and obtained their dephosphorylated RNA derivatives (SCRV-RNA-CIAP and VSV-
139 RNA-CIAP) through Calf Intestinal Alkaline Phosphatase (CIAP) treatment. Next, these RNAs
140 were transfected into MKC cells of *M. miiuy* and DF-1 cells of *G. gallus* respectively to detect the
141 dimerization form of IRF3. Results showed that virus RNA are more potent than dephosphorylated
142 virus RNA in activating IRF3 (Figure 1C and 1D). And further qPCR experiments showed that the
143 induction ability of IFN-1 by SCRV-RNA is significantly higher than that of SCRV-RNA-CIAP
144 (Figure 1E). These results indicate the presence of viral receptors in *M. miiuy* and *G. gallus* that
145 can recognize 5'ppp-RNA. Next, we compared the structural domains of human RIG-I and *M.*
146 *miiuy* MDA5 (mmiMDA5) and LGP2 (mmiLGP2) proteins, and observed that mmiLGP2 lacks
147 the CARD domain (Figure 1F). We next co-transfected mmiLGP2 plasmids or si-mmiLGP2 with
148 MDA5 plasmids into MKC cells. The results showed that mmiLGP2 can actively regulate
149 mmiMDA5's immune response to the SCRV virus (Figure 1G-1I), which further indicates that it
150 participates in antiviral immunity as an intermediate regulatory factor of MDA5 rather than a
151 downstream signal transmitter[7]. Therefore, these results prompted us to investigate whether
152 MDA5, a structurally similar homolog to RIG-I, can substitute for RIG-I in recognizing 5'ppp-
153 RNA in vertebrates without RIG-I (Figure 1J).
154

155 ***2.2 MDA5 promotes host antiviral innate immunity***

156 To further investigate the alternative immune function of MDA5, we first investigated the *M.*
157 *miiuy* MDA5-mediated signaling pathway in response to SCRV virus and double-stranded
158 mimetic poly(I:C)-HMW infection. Two siRNA molecules (si-MDA5-1 and si-MDA5-2) were

159 designed to assess the function of MDA5. si-MDA5-1 demonstrated higher inhibitory efficiency
160 compared to si-MDA5-2 (Figure 2A). Therefore, si-MDA5-1 (referred to as si-MDA5) was
161 selected for subsequent experiments. Subsequently, we constructed the MDA5 expression plasmid
162 and confirmed its protein overexpression efficiency and cytoplasmic localization (Figure 2B and
163 2C). Considering that mammalian MDA5 activates NF-κB and IRF3/IRF7 to induce IFNs, we
164 investigated whether *M. miiuy* MDA5 could impact these pathways. Dual-luciferase reporter
165 assays demonstrated that knockdown of MDA5 significantly inhibits NF-κB, IRF3, IRF7, and
166 IFN-1 reporter genes (Figure 2D). In addition, we investigated the role of MDA5 in regulating the
167 expression of IFN-stimulated genes (ISGs), which are crucial effectors. As shown in Figure 2E-
168 2G, we observed that knockdown or overexpression of MDA5 can significantly inhibit or promote
169 the expression levels of IFN-1, Mx1, ISG15, and Viperin upon SCRV infection or poly(I:C)-HMW
170 stimulation. To visually represent the biological significance of MDA5 in SCRV-induced host
171 cells, we utilized the virus plaque and qPCR methods to examine whether it could influence viral
172 replication. As demonstrated in Figure 2H-2K, knockdown of MDA5 led to a significant increase
173 in viral plaque formation and promoted SCRV replication in SCRV-infected cells, while
174 overexpression had the opposite effect. Next, we explored that how MDA5 conducts signal
175 transduction, and results showed that MDA5 is capable of binding not only to MAVS but also to
176 STING (Figure 2L and 2M). In our previous laboratory investigations, we have substantiated the
177 induction effect of STING on IFN under SCRV infection or poly(I:C) stimulation [24]. Under the
178 infection of SCRV virus, co-transfection of STING plasmids or si-STING with MDA5 plasmids
179 can significantly increase or decrease the induction of IFN-1, indicating the important role of
180 STING in MDA5-mediated immune transmission in response to RNA virus (Figure 2N and 2O).

181 Finally, through the determination of IRF3 dimer and IFN induction, our results showed that the
182 induction of antiviral innate immunity by SCRV-RNA depends on MDA5 (Figure 2P and 2Q).
183 Overall, these findings indicated that MDA5 plays a positive role in regulating the antiviral
184 responses of *M. miiuy*.
185
186 ***2.3 RD domain is required for MDA5 to recognize SCRV RNA***
187 We investigated whether *M. miiuy* MDA5, in the absence of RIG-I, can directly bind to the
188 RNA of SCRV. To address this question, we precipitated the MDA5 protein from SCRV-infected
189 MKC cells that were transfected with MDA5-Flag and pcDNA3.1-Flag. The bound RNA was then
190 amplified using SCRV-specific primers or β-actin primers as a control. Our results showed that
191 MDA5 interacted with SCRV RNA, while β-actin mRNA did not associate with MDA5 (Figure
192 3A). The C-terminal regulatory domain (RD) of human RIG-I binds to viral RNA in a
193 triphosphate-dependent manner, to determine if the RD domain of *M. miiuy* MDA5 has similar
194 functions, we generated truncated mutations called MDA5-ΔRD and Western blot analysis
195 confirmed the expression of MDA5 and MDA5-ΔRD plasmids (Figure 3B). We subsequently
196 noted that MDA5-ΔRD exhibited an inability to interact with SCRV RNA, which was supported
197 by the loss of its immunological capability in inhibiting SCRV viral replication (Figure 3C-3E).
198 We also examined the effects of MDA5 and MDA5-ΔRD on antiviral factors in both uninfected,
199 SCRV-infected, and poly(I:C)-HMW-stimulated MKC cells. In the absence of infection,
200 overexpression of both MDA5 and MDA5-ΔRD stimulated the expression of antiviral genes
201 (Figure 3F-3I). However, when cells were infected or stimulated with SCRV or poly(I:C)-HMW,
202 only the overexpression of MDA5, not MDA5-ΔRD, significantly increased the expression of

203 antiviral genes (Figure 3F-3I). In summary, these findings provided evidence that MDA5 may
204 recognize SCRV RNA through its RD domain.
205
206 ***2.4 MDA5 recognizes 5'ppp-RNA in M. miiuy and G. gallus***
207 To provide specific evidence of MDA5 recognition of 5'ppp-RNA in *M. miiuy*, we
208 synthesized 67 nt 5'ppp-SCRV from the SCRV virus and through in vitro transcription using T7
209 polymerase. As a positive control capable of binding to the mmiMDA5 receptor, 112 bp dsRNA
210 from the MDA5 gene sequence was also generated. Gel analysis and nuclease sensitivity
211 confirmed the generation of RNA products of the expected size (Figure 4A). The RNA pull-down
212 experiment showed that 5'ppp-SCRV can be recognized by mmiMDA5, similar to 112 bp blunt
213 end dsRNA (Figure 4B). Next, we transfected wild-type 5'ppp-SCRV and dephosphorylated
214 mutant SCRV RNAs (5'-OH-SCRV and 5'pppGG-SCRV) into MKC cells to detect the dimer of
215 IRF3, and found that the activation ability of 5'ppp-RNA on IRF3 depends on its triphosphate
216 structure (Figure 4C). in addition, knockdown of mmiMDA5 blocked the induction of IRF3 by
217 5'ppp-SCRV (Figure 4D). Furthermore, biotin-labeled 5'ppp-RNA captured mmiMDA5, while the
218 biotin-labeled mutant types (5'-OH-SCRV and 5'pppGG-SCRV) did not (Figure 4E). Additionally,
219 we purified recombinant MDA5 and MDA5-ΔRD of *M. miiuy* to conduct electrophoresis mobility
220 shift assay (EMSA) (Figure 4F). When recombinant mmiMDA5 was subjected to EMSA using a
221 biotin-labeled 5'ppp-SCRV probe, a clear complex was detected (Figure 4G). This complex
222 formation was inhibited by adding an excess of cold 5'ppp-SCRV but not 5'-OH-SCRV and
223 5'pppGG-SCRV, demonstrating the direct interaction between mmiMDA5 and 5'ppp-SCRV
224 (Figure 4G). However, 5'ppp-SCRV cannot bind to the MDA5-ΔRD (Figure 4H). Next, we

225 investigated whether *G. gallus* MDA5 (ggaMDA5) shares the ability to recognize 5'ppp-RNA
226 seen in fish. We synthesized 67 nt 5'ppp-VSV from the VSV virus and found that it is similar to
227 5'ppp-SCRV, binding to ggaMDA5 and activating IRF3 in a triphosphate-dependent manner (4I-
228 4M). Overall, our findings demonstrated that MDA5 detection of RNA in two RIG-I deficient
229 vertebrates (*M. miiuy and G. gallus*) is guided by the RNA 5'-triphosphate end and is disrupted
230 when RNA is capped at the 5'-triphosphate end or dephosphorylated.
231

232 ***2.5 Altered m^{6}A modification and expression of MDA5 upon SCRV infection***

233 As stated in the previous results, MDA5 has evolved to possess immune recognition abilities
234 that take over the role of RIG-I, significantly enhancing the host's ability to resist viral infections.
235 However, evolution is a continuous battle between hosts and viruses, viruses often evolve complex
236 escape mechanisms to evade immune surveillance and destruction, in which the m^{6}A modification
237 mechanism is an important way. To investigate the impact of SCRV infection on the overall
238 methylation dynamics of fish hosts, we utilized methylated RNA immunoprecipitation sequencing
239 (MeRIP-seq, GenBank accession number: PRJNA819945) to measure changes in m^{6}A
240 modification of host transcripts during SCRV infection (Figure 5A). From the results shown in
241 Figure 5B, we identified 3060 differentially m^{6}A methylated peaks (p-value < 0.05) and 2082
242 differentially expressed genes (p-value < 0.05) between the non-infected and SCRV-infected
243 group, indicating that infection significantly alters the m^{6}A modification of specific host
244 transcripts. It is worth noting that hyper-methylated m^{6}A peaks were also observed in the MDA5
245 mRNA transcripts during SCRV infection (fold change >1.5, $p < 0.05$), and the expression level of
246 MDA5 was higher in the infection group compared to the control group ($p < 0.05$). Further

247 analysis of the m^{6}A-seq data showed that MDA5 contained m^{6}A sites in the exon1 region which
248 were markedly higher in the infection group than that in the control group (Untreated VS SCRV: p
249 = 0.01) (Figure 5C). Next, we tested the concrete m^{6}A modification sites of MDA5 mRNA. We
250 used the SRAMP database to predict potential m^{6}A sites in MDA5-exon1 [25]. Four potential sites
251 were predicted and two specific primers were designed (Figure 5D), then m^{6}A quantitative real-
252 time PCR and semiquantitative PCR were performed. In line with the m^{6}A-seq data, the results
253 further confirmed that m^{6}A sites exactly exist in MDA5 exon1 (Figure 5E). After being infected
254 with SCRV or poly(I:C)-HMW, the methylation level of MDA5 increased in MKC cells, further
255 confirming the sequencing data (Figure 5F). We further inserted the MDA5-exon1 into pmirGLO,
256 and results showed that the infection of SCRV can reduce the luciferase activity of pmirGLO-
257 MDA5-exon1, and the use of cycloleucine (CL, an amino acid analogue that can inhibit m^{6}A
258 modification) hindered the degradation of MDA5-exon1 by SCRV, indicating that SCRV can
259 regulate MDA5 expression through a methylation mechanism (Figure 5G). MDA5 is classified as
260 an interferon-stimulated gene (ISG). Consistently, in spleen and kidney tissues infected with
261 SCRV, the expression level of MDA5 demonstrates fluctuation. (Figure 5H). We further explored
262 the mRNA and protein levels of MDA5 in MKC cells infected with SCRV and poly(I:C)-HMW
263 and found that their expression all first significantly increased and then returned to the normal
264 level (Figure 5I and 5J). Overall, our results suggested that the m^{6}A modification of MDA5 is
265 increased, and the expression level of MDA5 shows fluctuating changes upon SCRV infection.
266

267 ***2.6 m^{6}A-modification weakens MDA5 mRNA stability and antiviral ability***

268 SCRV infection can increase the methylation level of MDA5, and this mechanism is expected

269 to have a regulatory effect on MDA5. To investigate this, the regulatory effects of METTL3 and
270 METTL14, the main components of the methyltransferase complex, on MDA5 were explored.
271 Three siRNAs targeting METTL3 and METTL14 were designed, and si-METTL3-2 and si-
272 METTL14-3 showed higher knockdown efficiency (Figure 6A). METTL3 and METTL14-
273 overexpressing plasmids were also constructed, and the interaction between them confirmed their
274 cooperative role in m^6A modification (Figure 6B). Subsequently, the global m^6A levels were
275 measured in cells after knockdown or overexpression of METTL3 and METTL14. Consistent with
276 expectations, the knockdown of METTL3 and METTL14 significantly decreased the global m^6A
277 level, while their overexpression significantly increased the overall methylation level (Figure 6C).
278 To investigate their role in the process of virus infection, we used the virus plaque and qPCR
279 methods to explore whether it could affect SCRV replication. As shown in Figure 6D and 6E,
280 overexpression of METTL3 or METTL14 significantly enhances viral plaque formation and
281 promotes SCRV replication in SCRV-infected cells. And as m^6A writers, METTL3 and METTL14
282 can directly regulate the methylation level of MDA5 and induce MDA5 degradation by reducing
283 its mRNA stability (Figure 6F-6I). We further inserted the MDA5-exon1 into pmirGLO and
284 mVenus-C1 vector, and results showed that si-METTL3&14 can reduce the luciferase activity of
285 pmirGLO-MDA5-exon1, and METTL3&14 could suppress the levels of GFP, further indicating
286 the presence of methylation sites in MDA5-exon1 (Figure 6-figure supplement 1A and 1D). To
287 investigate the potential m^6A sites on MDA5-exon1, we constructed mutant MDA5-exon1 reporter
288 plasmids (Figure 5D and Figure 6-figure supplement 1B). As expected, our results showed that the
289 luciferase activity of wild-type pmirGLO-MDA5-exon1 reporter, but not of mutant pmirGLO-
290 MDA5-exon1 reporter, was markedly increased upon METTL3&14 knockdown (Figure 6-figure

291 supplement 1C). Furthermore, we found that the use of cycloleucine hindered the degradation of
292 MDA5 by METTL3 and METTL14, indicating that these proteins regulate MDA5 expression
293 through a methylation mechanism (Figure 6J and 6K). Additionally, MDA5 expression was
294 degraded by METTL3&14 in both SCRV-infected and uninfected groups (Figure 6L). To
295 investigate the impact of this mechanism on viral infection, we co-transfected METTL3&14 and
296 MDA5 plasmids and found that METTL3&14 partially suppressed the antiviral immune benefit of
297 MDA5 (Figure 6M-6O). Taken together, our data demonstrate that METTL3&14-mediated m^6A
298 methylation of MDA5 inhibits its mRNA stability and expression levels, thus suppressing the
299 antiviral capabilities of MDA5.
300
301 ***2.7 Detailed m^6A regulatory mechanism of MDA5***
302 The m^6A mechanism is jointly regulated by writers, erasers, and readers. The m^6A
303 modification of mRNA recruits m^6A-binding proteins (readers) which have the function of
304 recognizing m^6A sites and accelerating mRNA decay. In this study, we hypothesized that YTHDF
305 readers (YTHDF1, YTHDF2, and YTHDF3) may recognize m^6A-modified MDA5 and destabilize
306 it. We examined the binding ability of YTHDF proteins to MDA5 mRNA and found that YTHDF2
307 and YTHDF3 exhibited stronger binding compared to YTHDF1 (Figure 7A). We then designed
308 two siRNAs targeting YTHDF1, YTHDF2, and YTHDF3 respectively, and selected si-YTHDF1-
309 1, si-YTHDF2-si-2, si-YTHDF3-2 with better knockdown effects for subsequent experiments
310 (Figure 7B). Results showed that the knockdown or overexpression of YTHDF2 and YTHDF3 led
311 to the increase or decrease of the expression levels of MDA5, whereas YTHDF1 did not appear to
312 influence MDA5 expression (Figure 7C, 7D, Figure 7-figure supplement 1A and 1C). In addition,

overexpression of YTHDF2&3 can increase the luciferase activity of wild-type pmirGLO-MDA5-exon1 reporter, but not of mutant pmirGLO-MDA5-exon1 reporter (Figure 7-figure supplement 1B). We then found that si-METTL3&14 can counteract the negative impact of YTHDF2&3 on MDA5 mRNA, protein, and stability (Figure 7E and 7F). Since the m^6A mechanism is reversible, we then studied the regulation of MDA5 by two major erasers. Results showed that FTO, not ALKBH5, can upregulate MDA5 expression (Figure 7G). Moreover, the overexpression of FTO can reverse the inhibitory effect of YTHDF2&3 on MDA5 (Figure 7H and 7I). Taken together, these data suggested that through METTL3&14-m^6A-YTHDF2&3 regulatory network, m^6A can mediate the degradation of MDA5, and this process can be countered by FTO (Figure 7J).

3. Discussion

In this study, we have identified multiple independent loss events of RIG-I throughout vertebrate evolution. Specifically, we have observed at least three independent loss events in mammals, birds, and fish, respectively. Regarding the loss of RIG-I in avian species, previous studies have provided more comprehensive and accurate information than ours, indicating that birds have experienced more than 16 instances of RIG-I loss[10]. However, it should be noted that we have not found the loss of RIG-I in reptiles and amphibians (not displayed). But this does not imply that there has been no loss event among them, but rather, there is insufficient information regarding the genomes of reptiles and amphibians to draw the conclusions. As the abundance of genomic data continues to grow, there will be an increasing amount of evidence available to verify the presence or absence of RIG-I in these taxonomic groups. Additionally, the presence of RIG-I in current species does not guarantee that RIG-I loss has not occurred previously. For instance, our research has indicated that zebrafish may have experienced RIG-I loss. However, prior to the loss event, the zebrafish RIG-I has undergone repetitive events. These findings collectively highlight that the loss of RIG-I is not a random occurrence, but rather bears significant biological and evolutionary implications that deserve further investigation.

The evolutionary loss of RIG-I raises the question of a possible compensation of its function by other gene products. RIG-I deficiency instances in mammals were scarcer compared to those in fish and birds. Previous research has revealed that in *T. belangeri*, concurrent with the loss of RIG-I, both MDA5 and LGP2 have undergone notable positive selection, and MDA5 or MDA5/LGP2 could sense Sendai virus (an RNA virus posed as a RIG-I agonist) for inducing type I IFN. This proposed an immune substitution model for RIG-I deficiency in mammals, though

345 direct evidence of MDA5/LGP2 binding to 5’ppp-RNA was lacking. In this study, we
346 characterized the consequences resulting from the loss of RIG-I in the *M. miiuy* and *G. gallus* (two
347 representative species of vertebrates lacking RIG-I) and provided direct functional evidence for
348 the alternative immune recognition function of MDA5. SCRV and VSV belongs to the class of
349 rhabdovirus, which is a negative-strand virus with a non-segmented genome and initiate both
350 replication and transcription de novo leading to 5′-triphosphate RNA in the cytosol, was expected
351 to trigger an IFN response without the need for replication and presumed dsRNA formation[4].
352 Then, we synthesized 5’ppp-RNA probes from the SCRV and VSV genome sequences and
353 purified recombinant MDA5 of *M. miiuy* and *G. gallus*. Results demonstrated that MDA5 detect
354 the 5’ppp-RNA in *M. miiuy and G. gallus* and is disrupted when RNA is capped at the 5'-
355 triphosphate end or dephosphorylated. Furthermore, the recognition of RNA by MDA5 depends
356 on its RD domain, which not only indicates that the RD domain of MDA5 has evolved functions
357 similar to RD domain of RIG-I, but also excludes the possibility of MDA5 binding to 5’ppp-RNA
358 through intermediate ligands. Furthermore, in vertebrates that possess RIG-I, STING exclusively
359 binds to RIG-I rather than MDA5. However, similar to the interaction observed between MDA5
360 and STING in tree shrews and chickens that lacking RIG-I[8, 26], the MDA5 of *M. miiuy* can also
361 interact with STING protein, indicating that in vertebrates lacking RIG-I, MDA5 may utilize
362 STING to facilitate signal transduction in the antiviral response. Next, by linking the immune
363 replacement ability evolved by MDA5 with the common RIG-I loss event in vertebrates, we
364 propose a straightforward explanation for this evolutionary event: In the lengthy process of
365 vertebrate evolution, MDA5 gradually acquired new functionalities to effectively detect viruses
366 such as 5’ppp-RNAs, which were initially recognized by RIG-I. As a result, there was functional

367 redundancy of RIG-I, which eventually led to its gradual disappearance from the vertebrate
368 genome. This hypothesis is supported by two viewpoints: first, MDA5 and RIG-I can both
369 recognize overlapping viruses[27]; secondly, in fish without RIG-I deficiency, MDA5 has stronger
370 antiviral ability compared to RIG-I[28]. Finally, although MDA5 has a compensatory effect on RIG-
371 I, the absence of RIG-I may still have a significant impact on the immune system of vertebrates.
372 Ducks are often resistant to influenza viruses capable of killing chicken, and the loss of RIG-I in
373 chickens provides a plausible explanation for their increased susceptibility to influenza viruses
374 compared with ducks [29]. Furthermore, SCRV virus, the virus model used in this study, mainly
375 affects the *Siniperca chuatsi*, which is a fish species that also lacks RIG-I like *M. miiuy* [30].

376 Viruses are constantly co-evolving with hosts. Our available data suggested that the
377 vertebrate has evolved MDA5 with alternative functions to recognize and resist 5'ppp-RNA virus
378 in the absence of RIG-I. As a response, virus has also evolved to use the m^6A mechanism to evade
379 the host immune response. Previous study indicated that m^6A modification plays a crucial role in
380 maintaining immune homeostasis in the body[31]. During the infection process, the virus may
381 disrupt the m^6A level and disrupt the immune balance, thereby facilitating its own replication and
382 invasion. Viruses may utilize the m^6A mechanism in two ways to evade immunity. On the one
383 hand, many studies suggested a role for m^6A in shielding RNA species from detection by PRRs.
384 There are numerous viruses recognized in RIG-I dependent manner, but m^6A modification
385 increases the possibility of immune evasion. For example, the loss of m^6A site or removing m^6A
386 from human metapneumovirus may weaken its immune evasion ability, prevent it from evading
387 detection by RIG-I, and result in higher levels of IFN release[20]. Moreover, it has been reported
388 that the RNA containing m^6A modifications binds to RIG-I poorly, and it failed to trigger the RIG-

389 I conformational changes associated with downstream immune signals[32]. On the other hand, m^6A-
390 mediated viral strategies for inhibiting IFN induction pathways appear to exist. For instance,
391 following infection by human cytomegalovirus (HCMV), the IFN-β transcript was modified by
392 m^6A, and this methylation decreased its half-life, suggesting that HCMV can exploit this control
393 of IFN-β expression to facilitate its replication by increasing m^6A modification of the IFN-β
394 transcript and thus decreasing its production[33]. In another study, the m6A reader YTHDF3 could
395 restrain the type I IFN response and ISG expression by involving enhancement of FOXO3
396 translation in a m6A-independent mechanism, which acts as a negative regulator of immunity [19].
397 Moreover, previous study reports that IFN-α and IFN-β mRNA encoding cytokines that promote
398 IFN response are modified by m6A, and the loss of METTL3 and YTHDF2 could increase the
399 IFN expression and ISG activity [34]. In summary, viruses can utilize m^6A to evade the immune
400 response by shielding the recognition of RIG-I or reducing the host's immune reaction, thus
401 counteracting the host's defense mechanisms. In our previous study, we discovered that SCRV
402 infection can not only increase overall cellular methylation levels but also upregulate the
403 expression of METTL3, thereby suggesting its potential to regulate host gene expression through
404 the m^6A mechanism[35]. While changes in m^6A modification and the expression of m^6A-modified
405 transcripts are biologically relevant, identifying bona fide m^6A alterations during viral infection
406 will allow us to understand how m^6A modification of cellular mRNA is regulated. As our m^6A
407 change analysis pipeline controls for changes in gene expression, these data should represent true
408 changes in m^6A modification rather than changes in the expression of m^6A-modified transcripts. In
409 this study, we found that SCRV virus infection alters m^6A modification of specific cellular
410 transcripts, including MDA5. MDA5 plays a crucial role as a receptor in recognizing the SCRV

411 virus and controlling IFN activation. The aberrant m^6A levels of MDA5 subsequently affect the
412 expression of antiviral genes, thereby compromising its ability to mount an effective antiviral
413 immune response. It is plausible that SCRV also impacts the production of antiviral genes, such as
414 IFN-1 or other cytokines, by manipulating m^6A modification on the transcripts of cytokines or
415 molecules involved in their production. This interesting aspect warrants further investigation in
416 future research.

417 In this study, we demonstrated a co-evolutionary arms race between 5'ppp-RNA virus and
418 virus receptors. Specifically, we conducted an evolutionary analysis and provided functional
419 evidence to confirm that MDA5 of *M. miiuy* and *G. gallus* has acquired an additional function of
420 sensing 5'ppp-RNA, thus compensating for the loss of RIG-I. Additionally, we found that SCRV
421 infection can regulate the m^6A level of MDA5 in the *M. miiuy*, leading to its degradation and
422 subsequently affecting the immune response for immune evasion. Fish and birds, as the most
423 abundant aquatic and terrestrial vertebrates respectively, are also the two lineages with the most
424 frequent occurrence of RIG-I deficiency, the investigation of host-pathogen interactions of them
425 offers valuable insights into the ecological and evolutionary factors that contribute to the diversity
426 of the immune system.

427

428 ## 4. Materials and methods

429 ### *4.1 Ethics statement*

430 All animal experimental procedures were performed in accordance with the National
431 Institutes of Health's Guide for the Care and Use of Laboratory Animals, and the experimental
432 protocols were approved by the Research Ethics Committee of Shanghai Ocean University (No.
433 SHOU-DW-2018-047).

434

435 ### *4.2 Fish and challenge*

436 *M. miiuy* (~50 g) was obtained from Zhoushan Fisheries Research Institute, Zhejiang
437 Province, China. Fish was acclimated in aerated seawater tanks at 25℃ for six weeks before
438 experiments. The experimental procedure for SCRV infection was performed as described[36].
439 Briefly, In the SCRV injection group, fish was challenged with 200 μl SCRV at a multiplicity of
440 infection (MOI) of 5 through intraperitoneal. As a comparison, 200 μl of physiological saline was
441 used to challenge the individuals. Afterwards, fishes were respectively sacrificed at different time
442 point and the kidney and spleen tissues were collected for RNA extraction.

443

444 ### *4.3 Cell culture*

445 *M. miiuy* kidney cells (MKCs) and spleen cells (MPCs) are cell lines derived from the
446 kidney and spleen tissues of *M. miiuy* [37], with passages ranging from 20 to 40 times. MKC and
447 MPC cells were cultured in L-15 medium (HyClone) supplemented with 15% fetal bovine serum
448 (FBS; Gibco), 100 U/ml penicillin, and 100 μg/ml streptomycin at 26℃. Fish EPC cells
449 (Epithelioma papulosum cyprini cells) were maintained in medium 199 (Invitrogen) supplemented

450 with 10% FBS, 100 U/ml penicillin, and 100 mg/ml streptomycin at 26℃ in 5% CO_2. HEK293T
451 cells were cultured in DMEM (HyClone) supplemented with 10% FBS, 100 U/ml penicillin, and
452 100 mg/ml streptomycin at 37℃ in 5% CO_2. Chicken embryo fibroblast cells (DF-1) were
453 cultured in DMEM (HyClone) supplemented with 10% FBS, 100 U/ml penicillin, and 100 mg/ml
454 streptomycin at 39℃ in 5% CO_2.
455
456 ***4.4 Oligonucleotides***
457 The sequences of the 67 nt 5'ppp-SCRV or 5'ppp-VSV were derived from the 5' and 3'UTRs
458 of the VSV or SCRV genome as previously described[38], and the sequence of 112 bp dsRNA was
459 taken from the first 100 bp of the MDA5 gene of miiuy croaker flanked by 5'-gggaga and tctccc-
460 3'. These RNAs were synthesized by in vitro transcription using the Ribo RNAmax-T7 kit
461 (RiboBio). Biotin-labeled RNAs were transcribed in vitro using a Ribo RNAmax-T7 Biotin
462 Labeling Transcription Kit (RiboBio). For generating duplexes, RNA oligonucleotides were mixed
463 in hybridization buffer (20 mM Tris-HCl [pH 8.0], 1.5 mM $MgCl_2$, and 1.5 mM DTT), boiled for
464 1 min, and incubated at 37℃ for 1 h. For removal of 5'-triphosphates, 20 mg of RNA was treated
465 with 20 U Calf Intestinal Alkaline Phosphatase (CIAP, Invitrogen) for 2 h at 37℃ in the presence
466 of RNase inhibitor (Beyotime) and extracted with phenolchloroform. RNA molecules with a
467 terminal 5' m7G cap were synthesized by the incorporation of m7G cap analogue (Yeason) in the
468 transcription reactions. RNA was analysed on a denaturing 17% polyacrylamide, 7 M urea gel
469 following digestion with 50 ng/μl of RNase A (Beyotime) or 100 mU/μl of DNase I (Beyotime)
470 for 30 min.
471

472 ***4.5 Plasmids construction***

473 To construct Flag or Myc-tagged MDA5 (GeneBank: PP179381.1), MAVS, STING,
474 METTL3, METTL14, FTO, ALKBH5, YTHDF1, YTHDF2, and YTHDF3 expression plasmids,
475 their CDS sequences of the *M. miiuy* were amplified by PCR and then ligated into a pcDNA3.1
476 vector (Invitrogen), respectively. Then, MDA5-△RD were generated by PCR on the basis of
477 MDA5 plasmid. To construct MDA5-exon1 reporter vector, the exon1 region of *M. miiuy* MDA5
478 gene was amplified using PCR with the gene-specific primers and ligated into a pmir-GLO
479 luciferase reporter vector (Promega). Meanwhile, *M. miiuy* MDA5-exon1 were inserted into the
480 mVenus-C1 (Invitrogen), which included the sequence of enhanced GFP. For mutant reporter
481 vectors (MDA5-exon1-mut), adenosine (A) in the predicted m^6A motif was replaced by an uracil
482 (U) by using the Mut Express II Fast Mutagenesis Kit V2 (Vazyme) with specific primers). To
483 construct Flag-tagged MDA5 expression plasmid of *G. gallus*, the CDS sequence of MDA5 was
484 amplified by PCR and then ligated into a pcDNA3.1 vector (Invitrogen). The correct construction
485 of the recombinant plasmids was verified through Sanger sequencing and extracted using an
486 Endotoxin-Free Plasmid DNA Miniprep Kit (Tiangen, China) before using plasmids. The primers
487 were listed in Supplementary file 1.

488

489 ***4.6 Protein Purification and Analysis***

490 For protein purification, MDA5 plasmids with 6× His tag was constructed based on
491 pcDNA3.1. (His6)-Flag-tagged MDA5 of *M. miiuy* and *G. gallus* were transiently overexpressed
492 in 293T cells and lysed in a binding buffer (500 mM NaCl, 20 mM Tris/HCl [pH 7.4], 20 mM
493 Imidazole, and 1% Triton X-100) including protease inhibitor cocktail (Roche). The lysate was

494 incubated over night at 4℃ with anti-His beads (Solarbio). Anti-His beads were washed
495 subsequently with washing buffer (500 mM NaCl, 20 mM Tris/HCl [pH 7.4], 20 mM Imidazole,
496 and 1% Triton X-100). MDA5 proteins were eluted by an addtion of elution buffer (500 mM
497 NaCl, 20 mM Tris/HCl [pH 7.4], 500 mM Imidazole, and 1% Triton X-100) to the beads. Purity of
498 recombinant MDA5 was determined by SDS-PAGE separation.
499
500 ***4.7 RNA interference***
501 The MDA5-specific small interfering RNA (si-MDA5-1 and si-MDA5-2) sequences were 5'-
502 CGGACUACAUGCAGCGUAATT-3' and 5'-GACCAAUGAGAUUUCUAUGTT-3',
503 respectively. The LGP2-specific small interfering RNA (si-LGP2) sequence was 5'-
504 GGUUCACCUUGUAGAGCAATT-3'. The STING-specific small interfering RNA (si-STING)
505 sequence was 5'-ACGACAGCAUCCAUUUCUATT-3'. The METTL3-specific small interfering
506 RNA (si-METTL3-1, si-METTL3-2, and si-METTL3-3) sequences were 5'-
507 CAUCACAAACGAACUCAACTT-3', 5'- AACGUGGGCAAACUCUUUUTT-3' and 5'-
508 GAGAUUCUGGAACUACUUATT-3', respectively. The METTL14-specific small interfering
509 RNA (si-METTL14-1, si-METTL14-2, and si-METTL14-3) sequences were 5'-
510 GCUGGAAAUCGAGGAGAUATT-3', 5'- CCGTACGAAGAGGTGTACATT-3' and 5'-
511 GAGCCUCCCUUGGAAGAAUTT-3', respectively. The YTHDF1-specific small interfering
512 RNA (si-YTHDF1-1 and si-YTHDF1-2) sequences were 5'-AAAGACUUUGACUGGAACUTT-
513 3' and 5'-CAGUCGAUCAGAGACCUAATT-3', respectively. The YTHDF2-specific small
514 interfering RNA (si-YTHDF2-1 and si-YTHDF2-2) sequences were 5'-
515 GCAGGGUGUUUAUCAUCAATT-3', 5'- CUAUGCUCCCAGCUCAAUUTT-3', respectively.

516 The YTHDF3-specific small interfering RNA (si-YTHDF3-1 and si-YTHDF3-2) sequences were
517 5'-GGUGGACUACAAUGCCUAUTT-3' and 5'-UCUACAGUAACAGCUAUGGTT-3',
518 respectively. The scrambled control RNA sequences were 5' - UUCUCCGAACGUGUCACGUTT
519 - 3'. They were purchased from GenePharma (Shanghai, China).
520

521 ***4.8 Cells transfection***

522 Transient transfection of cells with siRNA was performed in 24-well plates using
523 Lipofectamine RNAiMAX (Invitrogen), and cells were transfected with DNA plasmids was
524 performed using Lipofectamine 3000 (Invitrogen) according to the manufacturer's instructions.
525 For functional analyses, the overexpression plasmid (500 ng per well) or control vector (500 ng
526 per well) and siRNA (100 nM) were transfected into cells in culture medium and then harvested
527 for further detection.
528

529 ***4.9 RNA extraction and quantitative real-time PCR***

530 Total RNA was extracted using the TRIzol Reagent (Invitrogen) and the cDNA was
531 synthesized using the FastQuant RT Kit (Tiangen) which contains DNase treatment of RNA to
532 eliminate genomic contamination, following the manufacturer's instructions. The expression
533 profiles of each gene were conducted by using the SYBR Premix Ex Taq™ (Takara), as
534 previously described. The quantitative real-time PCR was conducted in an Applied Biosystems®
535 QuantStudio 3 (Thermo Fisher Scientific). β-actin was used as internal controls. Primer sequences
536 are listed in Supplementary file 1.
537

538 ***4.10 Western blotting***

539 Cellular lysates were generated by using 1×SDS-PAGE loading buffer. Proteins were
540 extracted from cells and measured with the BCA Protein Assay kit (Vazyme), then subjected to
541 SDS-PAGE (10%) gel and transferred to PVDF (Millipore) membranes by semidry blotting (Bio-
542 Rad Trans Blot Turbo System). The membranes were blocked with 5% BSA. Protein was blotted
543 with different antibodies. The antibody against MDA5 was diluted at 1: 500 (Beyotime, Cat#
544 AF7164); The antibody against IRF3 was diluted at 1: 500 (Boster, Cat# BA4351-2); anti-Flag,
545 anti-Myc, anti-HA and anti-Tubulin monoclonal antibody were diluted at 1: 1,000 (Beyotime);
546 and HRP-conjugated anti-rabbit IgG or anti-mouse IgG (Abbkine) at 1: 5,000. The results were
547 the representative of three independent experiments. The immunoreactive proteins were detected
548 by using WesternBright^{TM} ECL (Advansta). The digital imaging was performed with a cold CCD
549 camera.

550

551 ***4.11 Dual-luciferase reporter assays***

552 For luciferase assays, MKC cells were co-transfected MDA5 expression plasmid, together
553 with NF-κB, IRF3, IRF7, or IFN-1 luciferase reporter genes, and the pRL-TK *Renilla* luciferase
554 reporter plasmid. For the detection of m^{6}A site, the wild or mutant of MDA5-exon1 luciferase
555 reporter was co-transfected si-METTL3, si-METTL14, si-YTHDF1, si-YTHDF2, si-YTHDF3 or
556 si-Ctrl into MKC cells. After 48 h transfection, the cells were collected and lysed for the reporter
557 luciferase activities measured by using a dual-luciferase reporter assay system (Promega). All the
558 luciferase activity values were gained against the *Renilla* luciferase control.

559

560 ***4.12 RNA binding protein immunoprecipitation (RIP)***

561 To identify whether MDA5 or MDA5-△RD can directly bind to SCRV viral RNA, MKC
562 cells (~2.0 × 10^7) were transfected with pcDNA3.1-Flag, pcDNA3.1-MDA5-Flag or pcDNA3.1-
563 MDA5-△RD-Flag and then infected with SCRV at an MOI of 5 for 24 h. In addition, to identify
564 whether YTHDF1, YTHDF2, and YTHDF3 can directly bind to MDA5, MKC cells were co-
565 transfected with pcDNA3.1-Flag, pcDNA3.1-YTHDF1/2/3-Flag. For RNA immunoprecipitation
566 (RIP) assays, MKC cells were harvested after 48 h transfection, and RIP assays were carried out
567 with Magna RIP RNA-Binding Protein Immunoprecipitation Kit (Millipore) and anti-Flag
568 antibody (Abcam) following the manufacturer's protocol. Then, the expression of target gene
569 SCRV-M, SCRV-G, β-actin, or MDA5 were detected by qRT-PCR analysis.

570

571 ***4.13 RNA Pull-Down assay***

572 Cytoplasmic extracts were prepared from 2 × 10^7 MKC cells transfected with mmiMDA5-Flag
573 (MDA5 of miiuy croaker) plasmids and 5 × 10^7 DF1 cells transfected with gga-MDA5-Flag
574 (MDA5 of chicken) plasmids. The extracts were incubated with biotinylated 5'ppp-RNA or
575 dsRNA and subjected to pull-down with streptavidin agarose beads (Geneseed), followed by
576 subsequent Coomassie bluestaining or SDS-PAGE analysis and immunoblotting with anti-Flag
577 antibody (Beyotime).

578

579 ***4.14 EMSA assay***

580 Recombinant MDA5 proteins were mixed with biotin-labeled oligonucleotides in a reaction
581 mixture (10 μl: 20 mM Tris-HCl pH 8.0, 1.5 mM $MgCl_2$, 1.5 mM DTT). After incubation at room

582 temperature for 15 min, the reaction mixtures were conducted on 6% non-denaturing
583 polyacrylamide gels and the EMSA was performed using Chemiluminescent EMSA Kit
584 (Beyotime).
585
586 ***4.15 MeRIP-seq assays and analysis***
587 Total RNA was isolated using TRIzol reagent. m^6A immunoprecipitation and library
588 preparation were performed following the manufacturer's protocol. Poly (A) RNA is purified from
589 50 μg total RNA using Dynabeads Oligo (dT) (Thermo Fisher) using two rounds of purification.
590 Then the poly(A) RNA was fragmented into small pieces using Magnesium RNA Fragmentation
591 Module (NEB) under 86℃ for 7 min. Then the cleaved RNA fragments were incubated for 2 h at
592 4℃ with m^6A-specific antibody (Synaptic Systems) in IP buffer (50 mM Tris-HCl, 750 mM NaCl
593 and 0.5% Igepal CA-630). For sequencing data analysis, we used HISAT2 to map reads to the
594 reference genome of *M. miiuy*. Mapped reads of IP and input libraries were provided for R
595 package exomePeak, which identifies m^6A peaks with bed or bigwig format that can be adapted
596 for visualization on the IGV software. The differentially expressed mRNAs were selected with
597 log2 (fold change) >1 or log2 (fold change) <-1 and p-value < 0.05 by R package edgeR. The
598 circus map of m^6A peaks in untreated and SCRV-infected spleen tissues of *M. miiuy* was showed
599 by TBtools[39].
600
601 ***4.16 MeRIP-qPCR***
602 Total RNA was extracted using TRIzol reagent (Invitrogen). Methylated m^6A RNA
603 immunoprecipitation (Me-RIP) was performed according to the protocol of EpiQuik™

604 CUT&RUN m^6A RNA Enrichment Kit (Epigentek). qPCR analysis of the methylated RNA was
605 performed to detect methylated MDA5 mRNA levels. Relative m^6A level for each transcript was
606 calculated as the percent of input in each condition normalized to that of the respective positive
607 control spike-in. Fold change of enrichment was calculated with mock samples normalized to 1 [40].
608

609 ***4.17 Total m^6A Quantification Assay***

610 Total RNA was extracted by the TRIzol Reagent (Invitrogen). Then, an EpiQuik m^6A RNA
611 Methylation Quantification Kit (EpiGentek) was used to detect the total m^6A level according to
612 the manufacturer's protocol. Briefly, positive control (PC), negative control (NC), and 200 ng
613 isolated mRNA were added to each well with the capture antibody. Next, the RNA was incubated
614 with m^6A antibody in wells, and m^6A content was quantified at a wavelength of 450 nm.
615

616 ***4.18 RNA stability assays***

617 Cells were treated with actinomycin D (5 μg/mL) and then collected at different time points.
618 RNA was extracted by TRIzol reagent (Invitrogen), and the mRNA levels were measured using
619 qRT-PCR.
620

621 ***4.19 Database mining and sequence analysis***

622 The species tree is constructed by submitting species names to the NCBI
623 (https://www.ncbi.nlm.nih.gov/Taxonomy/CommonTree/wwwcmt.cgi). In order to determine
624 whether there is RIG-I in vertebrates, we use *H. sapiens* and *D. rerio* RIG-I protein sequences to
625 TBLASTN the whole genome sequence of the species on the ensemble website

626 (http://www.ensemble.org/). In addition, in order to prevent the possibility of incomplete species
627 genome, we also used RIG-I protein sequences of *H. sapiens* and *D. rerio* to compare the
628 transcriptome and genome sequenced of the designated species on NCBI website
629 (http://www.ncbi.nlm.nih.gov/Genbank/). For further gene synteny analysis, RIG-I of *H. sapiens*,
630 *C. milii, D. rerio* were used as anchor sites. In order to identify the MDA5 and LGP2 from *M.*
631 *miiuy*, we used the homologues of zebrafish reported previously as queries to seek for the
632 transcriptome[41] and a chromosome-scale genome database[42] of *M. miiuy* by using local
633 TBLASTN and BLASTN programs, then the protein structures were predicted by SMART
634 website (http://smart.embl-heidelberg.de/).
635
636 ***4.20 Statistical analysis***
637 Data are expressed as the mean ± SE from at least three independent triplicated
638 experiments. . A two-sided Student's t test was used to evaluate the data. The relative gene
639 expression data was acquired using the $2^{-\Delta\Delta CT}$ method, and comparisons between groups were
640 analyzed by one-way analysis of variance (ANOVA) followed by Duncan's multiple comparison
641 tests. A value of $p < 0.05$ was considered significant.
642

Acknowledgements

This study was supported by the National Natural Science Foundation of China (31822057).

Author contributions

S.G. designed and performed experiments, analyzed the data, performed bioinformatics analysis, and wrote the manuscript. X.L. performed experiments and provided advice in experimental plans. W.Z. provided advice in experimental plans. T.X. directed all the experiments and participated in experimental design, data analyses, interpretation, and manuscript writing.

Declaration of interests

The authors declare no competing interests.

655 **References:**

656 1. Pichlmair, A. & Sousa, C. R. E. Innate recognition of viruses. *Immunity* **27**, 370-383 (2007).

657 2. Yoneyama, M., et al. Shared and unique functions of the DExD/H-box helicases RIG-I,
658 MDA5, and LGP2 in antiviral innate immunity. *Journal of Immunology* **175**, 2851-2858 (2005).

659 3. Kato, H., et al. Differential roles of MDA5 and RIG-I helicases in the recognition of RNA
660 viruses. *Nature* **441**, 101-105 (2006).

661 4. Hornung, V., et al. 5 '-triphosphate RNA is the ligand for RIG-I. *Science* **314**, 994-997
662 (2006).

663 5. Loo, Y.-M. & Gale, M., Jr. Immune Signaling by RIG-I-like Receptors. *Immunity* **34**, 680-
664 692 (2011).

665 6. Satoh, T., et al. LGP2 is a positive regulator of RIG-I- and MDA5-mediated antiviral
666 responses. *Proceedings of the National Academy of Sciences of the United States of America* **107**,
667 1512-1517 (2010).

668 7. Saito, T., et al. Regulation of innate antiviral defenses through a shared repressor domain in
669 RIG-I and LGP2. *Proceedings of the National Academy of Sciences of the United States of*
670 *America* **104**, 582-587 (2007).

671 8. Xu, L., et al. Loss of RIG-I leads to a functional replacement with MDA5 in the Chinese tree
672 shrew. *Proceedings of the National Academy of Sciences of the United States of America* **113**,
673 10950-10955 (2016).

674 9. Liang, B. & Su, J. Advances in aquatic animal RIG-I-like receptors. *Fish and shellfish*
675 *Immunology reports* **2**, 100012-100012 (2021).

676 10. Krchlikova, V., et al. Dynamic Evolution of Avian RNA Virus Sensors: Repeated Loss of

677 RIG-I and RIPLET. *Viruses-Basel* **15**, (2023).

678 11. Millet, J. K., Jaimes, J. A. & Whittaker, G. R. Molecular diversity of coronavirus host cell
679 entry receptors. *Fems Microbiology Reviews* **45**, (2021).

680 12. Walker, P. J., et al. ICTV Virus Taxonomy Profile: Rhabdoviridae 2022. *Journal of General*
681 *Virology* **103**, (2022).

682 13. Naz, S. S., Aslam, A. & Malik, T. An Overview of Immune Evasion Strategies of DNA and
683 RNA Viruses. *Infectious disorders drug targets* **21**, e300821192322 (2021).

684 14. Lou, X., Wang, J.-J., Wei, Y.-Q. & Sun, J.-J. Emerging role of RNA modification N6-
685 methyladenosine in immune evasion. *Cell Death & Disease* **12**, (2021).

686 15. Shi, H., Wei, J. & He, C. Where, When, and How: Context-Dependent Functions of RNA
687 Methylation Writers, Readers, and Erasers. *Molecular Cell* **74**, 640-650 (2019).

688 16. Zheng, G., et al. ALKBH5 Is a Mammalian RNA Demethylase that Impacts RNA
689 Metabolism and Mouse Fertility. *Molecular Cell* **49**, 18-29 (2013).

690 17. Jia, G., et al. N6-Methyladenosine in nuclear RNA is a major substrate of the obesity-
691 associated FTO. *Nature Chemical Biology* **7**, 885-887 (2011).

692 18. Wang, X., et al. N-6-methyladenosine-dependent regulation of messenger RNA stability.
693 *Nature* **505**, 117-+ (2014).

694 19. Zhang, Y., et al. RNA-binding protein YTHDF3 suppresses interferon-dependent antiviral
695 responses by promoting FOXO3 translation. *Proceedings of the National Academy of Sciences of*
696 *the United States of America* **116**, 976-981 (2019).

697 20. Lu, M., et al. N-6-methyladenosine modification enables viral RNA to escape recognition by
698 RNA sensor RIG-I. *Nature Microbiology* **5**, 584-+ (2020).

699 21. Wu, J., et al. N6-Methyladenosine Modification Opens a New Chapter in Circular RNA
700 Biology. *Frontiers in Cell and Developmental Biology* **9**, (2021).
701 22. Zhang, Q., & Gui, J. Virus genomes and virus-host interactions in aquaculture animals.
702 Science China-Life Sciences **58**, 156-169 (2015).
703 23. Chen, S. N., Zou, P. F. & Nie, P. Retinoic acid-inducible gene I (RIG-I)-like receptors (RLRs)
704 in fish: current knowledge and future perspectives. *Immunology* **151**, 16-25 (2017).
705 24. Chu, Q., Xu, T. J., Zheng, W. W., Chang, R. J. & Zhang, L. Long noncoding RNA AANCR
706 modulates innate antiviral responses by blocking miR-210-dependent MITA downregulation in
707 teleost fish, *Miichthys miiuy*. Science China-Life Sciences **64**, 1131-1148 (2021).
708 25. Zhou, Y., Zeng, P., Li, Y.-H., Zhang, Z. & Cui, Q. SRAMP: prediction of mammalian N-6-
709 methyladenosine (m(6)A) sites based on sequence-derived features. *Nucleic Acids Research* **44**,
710 (2016).
711 26. Xu, L., Yu, D., Fan, Y., Liu, Y.-P. & Yao, Y.-G. Evolutionary selection on MDA5 and LGP2 in
712 the chicken preserves antiviral competence in the absence of RIG-I. *Journal of Genetics and*
713 *Genomics* **46**, 499-503 (2019).
714 27. Schoggins, J. W., et al. A diverse range of gene products are effectors of the type I interferon
715 antiviral response (vol 472, pg 481, 2011). *Nature* **525**, (2015).
716 28. Wan, Q., Yang, C., Rao, Y., Liao, Z. & Su, J. MDA5 Induces a Stronger Interferon Response
717 than RIG-I to GCRV Infection through a Mechanism Involving the Phosphorylation and
718 Dimerization of IRF3 and IRF7 in CIK Cells. *Frontiers in Immunology* **8**, (2017).
719 29. Barber, M. R. W., Aldridge, J. R., Webster, R. G. & Magor, K. E. Association of RIG-I with
720 innate immunity of ducks to influenza. Proceedings of the National Academy of Sciences of the

721 United States of America **107**, 5913-5918 (2010).

722 30. Liu, X. Y., et al. Isolation, genomic and biological characterizations of a rhabdovirus from
723 mandarin fish (*Siniperca chuatsi*). Aquaculture 563, (2023).

724 31. Gan, L., Zhao, Y., Fu, Y. & Chen, Q. The potential role of m6A modifications on immune
725 cells and immunotherapy. *Biomedicine & Pharmacotherapy* **160**, (2023).

726 32. Durbin, A. F., Wang, C., Marcotrigiano, J. & Gehrke, L. RNAs Containing Modified
727 Nucleotides Fail To Trigger RIG-I Conformational Changes for Innate Immune Signaling. *Mbio* **7**,
728 (2016).

729 33. Rubio, R. M., Depledge, D. P., Bianco, C., Thompson, L. & Mohr, I. RNA m(6)A
730 modification enzymes shape innate responses to DNA by regulating interferon beta. *Genes &*
731 *Development* **32**, 1472-1484 (2018).

732 34. Winkler, R., et al. m(6)A modification controls the innate immune response to infection by
733 targeting type I interferons. *Nature Immunology* **20**, 173-+ (2019).

734 35. Geng, S., et al. The m6A Reader YTHDF2 Modulates Antiviral and Antibacterial Activity by
735 Suppressing METTL3 Methylation-Modified STING in Fish. *Journal of immunology (Baltimore,*
736 *Md. : 1950)* **210**, 653-667 (2023).

737 36. Chu, Q., Xu, T., Zheng, W., Chang, R. & Zhang, L. Long noncoding RNA MARL regulates
738 antiviral responses through suppression miR-122-dependent MAVS downregulation in lower
739 vertebrates. *Plos Pathogens* **16**, (2020).

740 37. Geng, S., Zheng, W., Zhao, Y. & Xu, T. FTO promotes innate immunity by controlling NOD1
741 expression via m6A-YTHDF2 manner in teleost. *Iscience* **25**, (2022).

742 38. Goulet, M.-L., et al. Systems Analysis of a RIG-I Agonist Inducing Broad Spectrum Inhibition

743 of Virus Infectivity. Plos Pathogens **9**, (2013).

744 39. Chen, C., et al. TBtools: An Integrative Toolkit Developed for Interactive Analyses of Big

745 Biological Data. *Molecular Plant* **13**, 1194-1202 (2020).

746 40. McIntyre, A. B. R., et al. Limits in the detection of m^6A changes using MeRIP/m^6A-seq.

747 Scientific Reports **10**, (2020).

748 41. Che, R. B., Sun, Y. Y., Sun, D. Q. & Xu, T. J. Characterization of the Miiuy Croaker

749 (Miichthys miiuy) Transcriptome and Development of Immune-Relevant Genes and Molecular

750 Markers. *Plos One* **9**, (2014).

751 42. Xu, T., Li, Y., Zheng, W., & Sun, Y. A chromosome-level genome assembly of the miiuy

752 croaker (*Miichthys miiuy*) using nanopore sequencing and Hi-C. *Aquaculture and Fisheries*.

753 10.1016/j.aaf.2021.06.001 (2021).

754

Figure Legends:

Figure 1. A genetic compensation response model for RIG loss. (A) Loss of RIG-I in vertebrates. Each branch tip represents one species. Red lines show lineages where loss of RIG-I. The red circle indicates the occurrence of an independent loss event. Branch lengths scale in millions of years (MYA). (B) Comparative analysis of gene synteny of RIG-I in vertebrate genomes. (C and D) SCRV-RNA and VSV-RNA were extracted from SCRV and VSV virus and dephosphorylated them with Calf Intestinal Alkaline Phosphatase (CIAP). Then, MKC cells were transfected with SCRV-RNA and SCRV-RNA+CIAP, and DF-1 cells were transfected with VSV-RNA and VSV-RNA+CIAP. IRF3 dimerization was analyzed by native gel electrophoresis. (E) MKC cells were transfected with different concentrations of SCRV-RNA and SCRV-RNA+CIAP, then the expression of IFN-1 was detected by qRT-PCR. As a control, the expression level of IFN-1 in MKC cells transfected with the same volume of water was set to "1". (F) Predicted protein structures of MDA5 and LGP2 of *M. miiuy* and RIG-I of *H. sapiens*. (G) The expression of MDA5 and LGP2 plasmids of *M. miiuy* were detected by Western Blot. (H) MKC cells were co-transfected with MDA5 plasmids and LGP2 plasmids for 24 h and then treated with SCRV (MOI = 5) for 24 h. The expression of IFN-1 was determined by qPCR. (I) MKC cells were co-transfected with MDA5 plasmids and si-LGP2 for 24 h and then treated with SCRV (MOI = 5) for 24 h. The expression of LGP2 and IFN-1 was determined by qPCR. (J) A genetic compensation response model for RIG loss. All data presented as the means ± SE from at least three independent triplicated experiments. **, $p < 0.01$ versus the controls.

Figure 2. MDA5 promotes host antiviral innate immunity. (A) Silence efficiency of si-MDA5

777 measured by qRT-PCR and Western blotting. Two siRNAs of MDA5 were transfected into MPC
778 cells for 48 h respectively. (B) MKC cells were transfected with MDA5 plasmids for 48 h, then
779 the overexpression efficiency was detected through MDA5 endogenous antibodies. (C)
780 Subcellular localization of MDA5 in MKCs by immunofluorescence. (D) MDA5 knockdown
781 suppresses NF-κB, IRF3, IRF7, and IFN-1 signaling. MPC cells were transfected with pRL-TK
782 Renilla luciferase plasmid, luciferase reporter genes, together with MDA5 expression plasmid. At
783 48 h post-transaction, the luciferase activity was measured and normalized to renilla luciferase
784 activity. (E) Knockdown of MDA5 attenuates the expression of antiviral genes. MPC cells were
785 transfected with si-Ctrl or si-MDA5 for 24 h and then treated with SCRV (MOI =5) or poly(I:C)-
786 HMW for 24 h. The expression of IFN-1, Mx1, ISG15, and Viperin were determined by qPCR. (F
787 and G) Overexpression of MDA5 promotes the expression of antiviral genes. MKC cells were
788 transfected with vector or MDA5 expression plasmids for 24 h and then treated with SCRV (MOI
789 = 5) or poly (I:C)-HMW for 24 h. The expression of MDA5 (F), and antiviral genes, including
790 IFN-1, Mx1, ISG15, and Viperin (G) were determined by qPCR. (H and J) MPC cells transfected
791 with si-Ctrl or si-MDA5 and MKC cells transfected with pcDNA3.1 vector or MDA5 plasmid 24
792 h and then treated with SCRV at the dose indicated for 48 h. Then, cell monolayers were fixed
793 with 4% paraformaldehyde and stained with 1% crystal violet. (I and K) MDA5 inhibits SCRV
794 replication. MPC cells were transfected with si-Ctrl or si-MDA5 and MKC cells were transfected
795 with pcDNA3.1 vector or MDA5 expression plasmid for 24 h, then infected with SCRV (MOI =
796 5) for 12, 24, or 48 h. The qPCR analysis was conducted for SCRV-M and SCRV-G RNA levels.
797 (L and M) MDA5 immunoprecipitates with MAVS (L) and STING (M). EPC cells (~ 1×10^7) were
798 co-transfected with MAVS-Myc or STING-Myc and MDA5-Flag expression plasmids for 24 h,

799 followed by immunoprecipitation (IP) with anti-Myc. (N and O) MKC cells were transfected with
800 MDA5 plasmids and STING plasmids (N) or si-STING (O) for 24 h and then treated with SCRV
801 (MOI = 5) for 24 h. The expression of IFN-1 was determined by qPCR. (P and Q) MKC cells were
802 transfected with si-MDA5 for 24 h and then transfected with SCRV-RNA for 24 h, then the IRF3
803 dimerization and IFN-1 levels were analyzed by native gel electrophoresis (P) and qPCR (Q),
804 respectively. All data presented as the means ± SE from at least three independent triplicated
805 experiments. **, $p < 0.01$; *, $p < 0.05$ versus the controls.
806
807 **Figure 3. RD domain is required for MDA5 to recognize SCRV RNA.** (A) The association of
808 MDA5 proteins with SCRV. (B) Schematics and expression of MDA5 and truncated MDA5
809 (MDA5-△RD). (C) The association of MDA5 and MDA5-△RD proteins with SCRV. (D) MKC
810 cells transfected with pcDNA3.1 vector, MDA5, or MDA5-△RD plasmids for 24 h and then
811 treated with SCRV at the dose indicated for 48 h. Then, cell monolayers were fixed with 4%
812 paraformaldehyde and stained with 1% crystal violet. (E) MKC cells were transfected with
813 pcDNA3.1 vector, MDA5 or MDA5-△RD expression plasmids for 24 h, then infected with SCRV
814 for 24 h, then the qPCR analysis was conducted for SCRV-M and SCRV-G RNA levels. (F-I)
815 Expression of IFN-1 (F), Mx1 (G), ISG15 (H), and Viperin (I) in Mock-infected, SCRV-infected,
816 and poly(I:C)-HMW-stimulated MKC cells transfected with pcDNA3.1 vector, MDA5, or MDA5-
817 △RD expression plasmids. All data presented as the means ± SE from at least three independent
818 triplicated experiments. **, $p < 0.01$ versus the controls.
819
820 **Figure 4. MDA5 recognizes 5'ppp-RNA in *M. miiuy and G. gallus*.** (A) Schematic

821 representation of 5’ppp-SCRV and dsRNA. The product of in vitro transcription runs as a single
822 product degraded by RNase I. (B) Pull-down of biotinylated or non-biotinylated dsRNA and
823 5’ppp-SCRV by mmiMDA5. MKC cells were transfected with mmiMDA5-Flag plasmid, and the
824 input and immunoprecipitated MDA5 proteins were analyzed by Western blot. (C) MKC cells
825 were transfected with 5’ppp-SCRV, 5’OH-SCRV (5’ppp-SCRV dephosphorylated by CIAP), or
826 5’pppGG-SCRV (5’ppp-SCRV capped by m7G cap analog), then IRF3 dimerization was analyzed
827 by native gel electrophoresis. (D) WT and si-MDA5 MKC cells were transfected with 5’ppp-
828 SCRV and poly(I:C)-HMW, then IRF3 dimerization was analyzed by native gel electrophoresis.
829 (E) The cytoplasmic fraction of MKC cells transfected with Flag-tagged mmiMDA5 was
830 incubated with biotinylated 5’ppp-SCRV, 5’OH-SCRV, or 5’pppGG-SCRV. RNA-protein
831 complexes were pulled down using streptavidin affinity beads. Input and pull-down samples were
832 analyzed by SDS-PAGE and immunoblotting using anti-Flag antibody. (F) Purity of recombinant
833 mmiMDA5 and mmiMDA5-△RD were determined by SDS-PAGE and immunoblotting using
834 anti-His antibody. (G) EMSA of 5’ppp-SCRV with mmiMDA5. For binding competition,
835 indicated non-biotinylated RNAs (50-fold molar excess over the probe) were included. The
836 asterisk marks the binding bands between mmiMDA5 protein and different RNA probes. (H)
837 EMSA of 5’ppp-SCRV with mmiMDA5 or mmiMDA5-△RD. The asterisk marks the binding
838 bands between mmiMDA5 or mmiMDA5-△RD proteins and 5’ppp-SCRV RNA probes. (I)
839 Schematic representation of 5’ppp-VSV. The product of in vitro transcription runs as a single
840 product degraded by RNase I. (J) Pull-down of dsRNA and 5’ppp-VSV by ggaMDA5. DF-1 cells
841 were transfected with ggaMDA5-Flag plasmids, and the input and immunoprecipitated MDA5
842 proteins were analyzed by Western blot. (K) DF-1 cells were transfected with 5’ppp-VSV, 5’OH-

843 VSV (5'ppp-VSV dephosphorylated by CIAP), or 5'pppGG-VSV (5'ppp-VSV capped by m7G
844 cap analog), then IRF3 dimerization was analyzed by native gel electrophoresis. (L) The
845 cytoplasmic fraction of DF-1 cells transfected with Flag-tagged ggaMDA5 was incubated with
846 biotinylated 5'ppp-VSA, 5'OH-VSV, or 5'pppGG-RNA. RNA-protein complexes were pulled
847 down using streptavidin affinity beads. Input and pull-down samples were analyzed by SDS-
848 PAGE and immunoblotting using anti-Flag antibody. (M) EMSA of 5'ppp-RNA with ggaMDA5.
849 For binding competition, indicated non-biotinylated RNAs (50-fold molar excess over the probe)
850 were included. The asterisk marks the binding bands between ggaMDA5 protein and different
851 RNA probes.
852
853 **Figure 5. Increased m^{6}A modification and expression of MDA5 upon SCRV infection.** (A)
854 Schematic of the MeRIP-seq protocol used to identify differential m^{6}A methylation following
855 infection of *M. miiuy* spleen tissues with SCRV. (B) Circos plots showing differentially m^{6}A-
856 methylated peaks identified from normal and SCRV-infected spleen tissues of *M. miiuy*. The green
857 and red lines on the innermost ring represented the m^{6}A peaks identified from normal and SCRV-
858 infected spleen tissues of *M. miiuy* respectively. The orange lines represent the log2 fold change
859 values for each differentially m^{6}A peak. The blue spots represent the fold change of gene
860 expression. Chromosomes were shown on the outermost ring, the ruler on which represented the
861 physical distance is in millions of bases (Mb). (C) The m^{6}A abundance in MDA5 mRNA
862 transcripts detected by MeRIP-seq, the m^{6}A peak of MDA5 is circled in the green box. (D) The
863 exon1 sequence of MDA5 was submitted to the SRAMP website, and then the predicted m^{6}A site
864 was displayed. Four predicted methylation sites located on the exon1 of MDA5 were marked by

865 red box, then we designed two m^6A specific primers (MDA5-m^6A-1 and MDA5-m^6A-2). (E) m^6A
866 abundance on MDA5 exon1 detected by MeRIP-qPCR and emiquantitative PCR in MKC cells.
867 (F) MeRIP-qPCR analysis of relative m^6A level of MDA5 in Mock, SCRV-infected, and
868 poly(I:C)-HMW-stimulated MKC cells. (G) Relative luciferase activity of pmirGLO-MDA5-
869 exon1 firefly luciferase reporters in Mock and SCRV-infected (MOI = 5) MKC cells that treated
870 with DMSO or Cycloleucine (CL, 20 mM). (H) mRNA levels of MDA5 in spleen and kidney
871 tissues measured by qRT-PCR at indicated time after SCRV infection (MOI = 5). (I and J) mRNA
872 and protein levels of MDA5 in MKC cells measured by qRT-PCR and Western blotting at
873 indicated time after SCRV infection (MOI = 5) (I) and poly(I:C)-HMW stimulation (J). All data
874 presented as the means ± SE from at least three independent triplicated experiments. **, $p < 0.01$
875 versus the controls.
876
877 **Figure 6. m^6A-modification weakens MDA5 mRNA stability and antiviral ability.** (A) Silence
878 efficiency of si-METTL3 and si-METTL14 measured. Three siRNAs of METTL3 and METTL14
879 were transfected into MPC cells for 48 h respectively. (B) METTL3 immunoprecipitates with
880 METTL14. EPC cells (1×10^7) were co-transfected with METTL3-Myc and METTL14-Flag
881 expression plasmids for 24 h, followed by immunoprecipitation (IP) with anti-Myc. (C) METTL3
882 and METTL14 significantly increased the m^6A content. MPCs were transfected with si-Ctrl or si-
883 METTL3 or si-METTL14 and MKCs were transfected with vector or METTL3 or METTL14
884 plasmids for 48 h, then the m^6A level was measured by colorimetry. (D) METTL3 and METTL14
885 overexpressed MKC cells seeded in 48-well plates overnight were treated with SCRV at the dose
886 indicated for 48 h. Then, cell monolayers were fixed with 4% paraformaldehyde and stained with

887 1% crystal violet. (E) MKC cells were transfected with pcDNA3.1 vector and METTL3 or
888 METTL14 expression plasmid for 24 h, then infected with SCRV (MOI = 5) for 24 h. The qPCR
889 analysis was conducted for SCRV-M and SCRV-G RNA levels. (F) The m^6A level alteration of
890 MDA5 upon METTL3 or METTL14 knockdown or overexpression was examined by MeRIP-
891 qPCR. MPC cells were transfected with si-Ctrl or si-METT3 and MKC cells were transfected with
892 vector or METTL3 or METTL14 plasmids for 48 h. (G and H) MPC cells were transfected with
893 si-Ctrl, si-METTL3 or METTL14 and MKC cells were transfected with vector, METTL3, or
894 METTL14 plasmids for 48 h, the expression of MDA5 was detected by qRT-PCR and Western
895 blotting. (I) MPC cells were transfected with si-Ctrl, si-METTL3, or si-METTL14, and MKC cells
896 were transfected with vector, METTL3, or METTL14 plasmids, then 5 μg/ml actinomycin D was
897 added to the cells for 0 h, 2 h, and 4 h. The half-life of MDA5 was analyzed by qRT-PCR. (J)
898 MKC cells were transfected with vector or METTL3&14 plasmids for 24 h and then treated with
899 Cycloleucine (CL) for 24 h in a final concentration of 20 mM. The expression of MDA5 was
900 detected by qRT-PCR and Western blotting. (K) MKC cells were transfected with vector or
901 METTL3&14 plasmids for 24 h and then treated with CL for 24 h at 20 mM, then 5 μg/ml
902 actinomycin D was added to the cells for 0 h, 2 h, and 4 h. The half-life of MDA5 was analyzed
903 by qRT-PCR. (L) MKC cells were transfected with vector or METTL3&14 plasmids for 24 h and
904 stimulated with SCRV (MOI = 5) for 24 h, then the expression of MDA5 was detected by qRT-
905 PCR and Western blotting. (M) MKC cells seeded in 48-well plates overnight were transfected
906 with MDA5 or MDA5+METTL3&14 plasmids for 48 h, then the expression of MDA5 was
907 detected by qRT-PCR. (N) MKC cells seeded in 48-well plates overnight were transfected with
908 MDA5 or MDA5+METTL3&14 plasmids were treated with SCRV at the dose indicated for 48 h.

909 Then, cell monolayers were fixed with 4% paraformaldehyde and stained with 1% crystal violet.
910 (O) MKC cells were transfected with MDA5 or MDA5 + METTL3&14 plasmids for 24 h, then
911 infected with SCRV (MOI = 5) for 24 h. The qPCR analysis was conducted for SCRV-M and
912 SCRV-G RNA levels. All data presented as the means ± SE from at least three independent
913 triplicated experiments. **, $p < 0.01$; *, $p < 0.05$ versus the controls.
914
915 **Figure 7. Detailed m^{6}A regulatory mechanism of MDA5.** (A) The binding relationship between
916 YTHDF1, YTHDF2, or YTHDF3 and MDA5 mRNA was validated using a RIP assay. MKC cells
917 were transfected with YTHDF1-Flag, YTHDF2-Flag, YTHDF3-Flag, or pcDNA3.1-Flag for 48 h.
918 (B) SiRNA silencing effect test of YTHDF1, YTHDF2, and YTHDF3. MPC cells were transfected
919 with si-YTHDF1, si-YTHDF2, or si-YTHDF3 for 48 h. (C and D) MPC cells were transfected
920 with si-YTHDF1, si-YTHDF2, si-YTHDF3 or si-Ctrl (C), and MKC cells were transfected with
921 YTHDF1, YTHDF2, YTHDF3 or vector for 48 h (D), then the expression of MDA5 was detected
922 by qRT-PCR and Western blotting. (E) Relative mRNA and protein levels of MDA5 in MKC cells
923 after co-transfected with YTHDF2&3 plasmids and si-METTL3&14 by qPCR and western blot
924 assays. (F) MKC cells were transfected with YTHDF2&3 plasmids and si-METTL3&14, then 5
925 μg/ml actinomycin D was added to the cells for 0 h, 2 h, and 4 h. The half-life of MDA5 was
926 analyzed by qRT-PCR. (G) MKC cells were transfected with vector, FTO, ALKBH5 plasmids for
927 48 h, then the expression of MDA5 was detected by qRT-PCR and Western blotting. (H) Relative
928 mRNA and protein levels of MDA5 in MKC cells after co-transfected with YTHDF2&3 plasmids
929 and FTO plasmids by qPCR and western blotting. (I) MKC cells were transfected with
930 YTHDF2&3 plasmids and FTO plasmids, then 5 μg/ml actinomycin D was added to the cells for 0

931 h, 2 h, and 4 h. The half-life of MDA5 was analyzed by qRT-PCR. (J) Schematic diagram of arms
932 race between MDA5 and 5'ppp-RNA virus in *M. miiuy*.
933

934 ## Supporting Information

935 **Supplementary file 1.** PCR primer information in this study.
936

937 **Figure 6-figure supplement 1. The regulation of m^{6}A writers (METTL3&14) to the MDA5-**
938 **exon1.** (A) Relative luciferase activity of pmirGLO-MDA5-exon1 firefly luciferase reporters in
939 MPC cells transfected with si-Ctrl, si-METTL3 or si-METTL14. (B) Schematic diagram of m^{6}A
940 site mutation on exon1 of MDA5. 'A' in the predicted methylation motif was replaced by 'U'. (C)
941 Relative luciferase activity of wild-type or mutant pmirGLO-MDA5-exon1 firefly luciferase
942 reporter in MPC cells transfected with si-Ctrl or si-METTL3&14. (D) METTL3 and METTL14
943 could downregulate GFP expression of mVenus-MDA5-exon1. EPC cells were co-transfected with
944 the mVenus-MDA5-exon1 and vector, METTL3 or METTL14 plasmids. At 48 h post-transfection,
945 the fluorescence intensity and the GFP expression were evaluated by enzyme-labeled instrument
946 and western blotting, respectively. All data presented as the means ± SE from at least three
947 independent triplicated experiments. **, $p < 0.01$ versus the controls.
948

949 **Figure 7-figure supplement 1. The regulation of YTHDF readers (YTHDF1&2&3) to the**
950 **MDA5-exon1.** (A) Relative luciferase activity of pmirGLO-MDA5-exon1 firefly luciferase
951 reporters in MPC cells transfected with si-Ctrl, si-YTHDF1, si-YTHDF2 or si-YTHDF3. (B)
952 Relative luciferase activity of wild-type or mutant pmirGLO-MDA5-exon1 plasmids in MPC cells

953 transfected with si-Ctrl or si-YTHDF2&3. (C) YTHDF2 and YTHDF3 could downregulate GFP
954 expression of mVenus-MDA5-exon1. EPC cells were co-transfected with the mVenus-MDA5-
955 exon1 and vector, YTHDF1, YTHDF2 or YTHDF3 plasmids. At 48 h post-transfection, the
956 fluorescence intensity and the GFP expression were evaluated by enzyme-labeled instrument and
957 western blotting, respectively. All data presented as the means ± SE from at least three
958 independent triplicated experiments. **, $p < 0.01$ versus the controls.
959

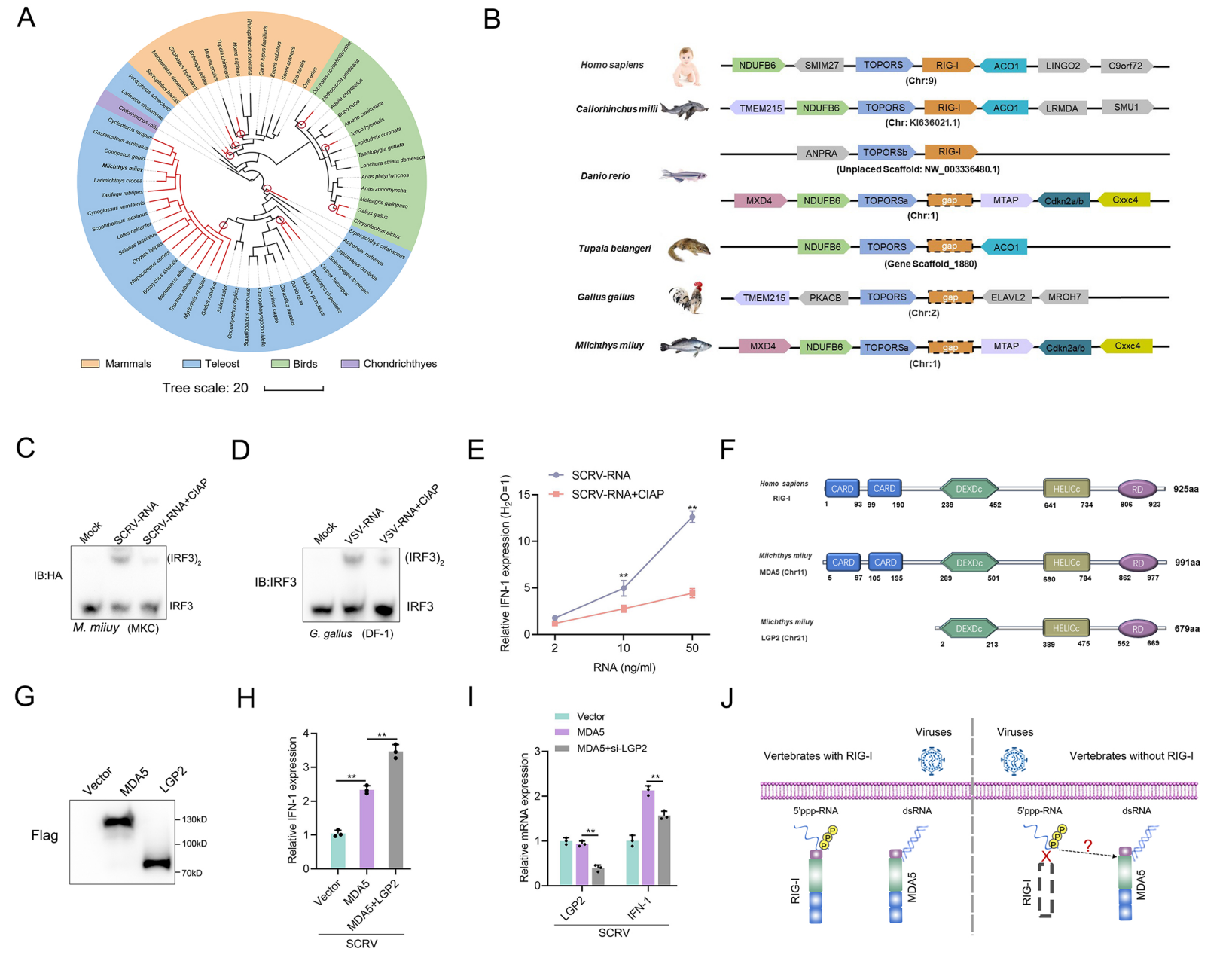
A
Mammals
Teleost
Birds
Chondrichthyes
Tree scale: 20
B
Homo sapiens
NDUFB6
SMIM27
TOPORS
RIG-I
ACO1
LINGO2
C9orf72
(Chr:9)
Callorhinchus milii
TMEM215
NDUFB6
TOPORS
RIG-I
ACO1
LRMDA
SMU1
(Chr: KI636021.1)
Danio rerio
ANPRA
TOPORSb
RIG-I
(Unplaced Scaffold: NW_003336480.1)
MXD4
NDUFB6
TOPORSa
gap
MTAP
Cdkn2a/b
Cxxc4
(Chr:1)
Tupaia belangeri
NDUFB6
TOPORS
gap
ACO1
(Gene Scaffold_1880)
Gallus gallus
TMEM215
PKACB
TOPORS
gap
ELAVL2
MROH7
(Chr:Z)
Miichthys miiuy
MXD4
NDUFB6
TOPORSa
gap
MTAP
Cdkn2a/b
Cxxc4
(Chr:1)
C
Mock
SCRV-RNA
SCRV-RNA+CIAP
IB:HA
(IRF3)2
IRF3
M. miiuy (MKC)
D
Mock
VSV-RNA
VSV-RNA+CIAP
IB:IRF3
(IRF3)2
IRF3
G. gallus (DF-1)
E
SCRV-RNA
SCRV-RNA+CIAP
Relative IFN-1 expression (H2O=1)
RNA (ng/ml)
F
Homo sapiens
RIG-I
CARD
CARD
DEXDc
HELICc
RD
925aa
Miichthys miiuy
MDA5 (Chr11)
991aa
Miichthys miiuy
LGP2 (Chr21)
679aa
G
Vector
MDA5
LGP2
Flag
130kD
100kD
70kD
H
Relative IFN-1 expression
Vector
MDA5
MDA5+LGP2
SCRV
I
Vector
MDA5
MDA5+si-LGP2
Relative mRNA expression
LGP2
IFN-1
SCRV
J
Viruses
Vertebrates with RIG-I
Viruses
Vertebrates without RIG-I
5'ppp-RNA
dsRNA
RIG-I
MDA5

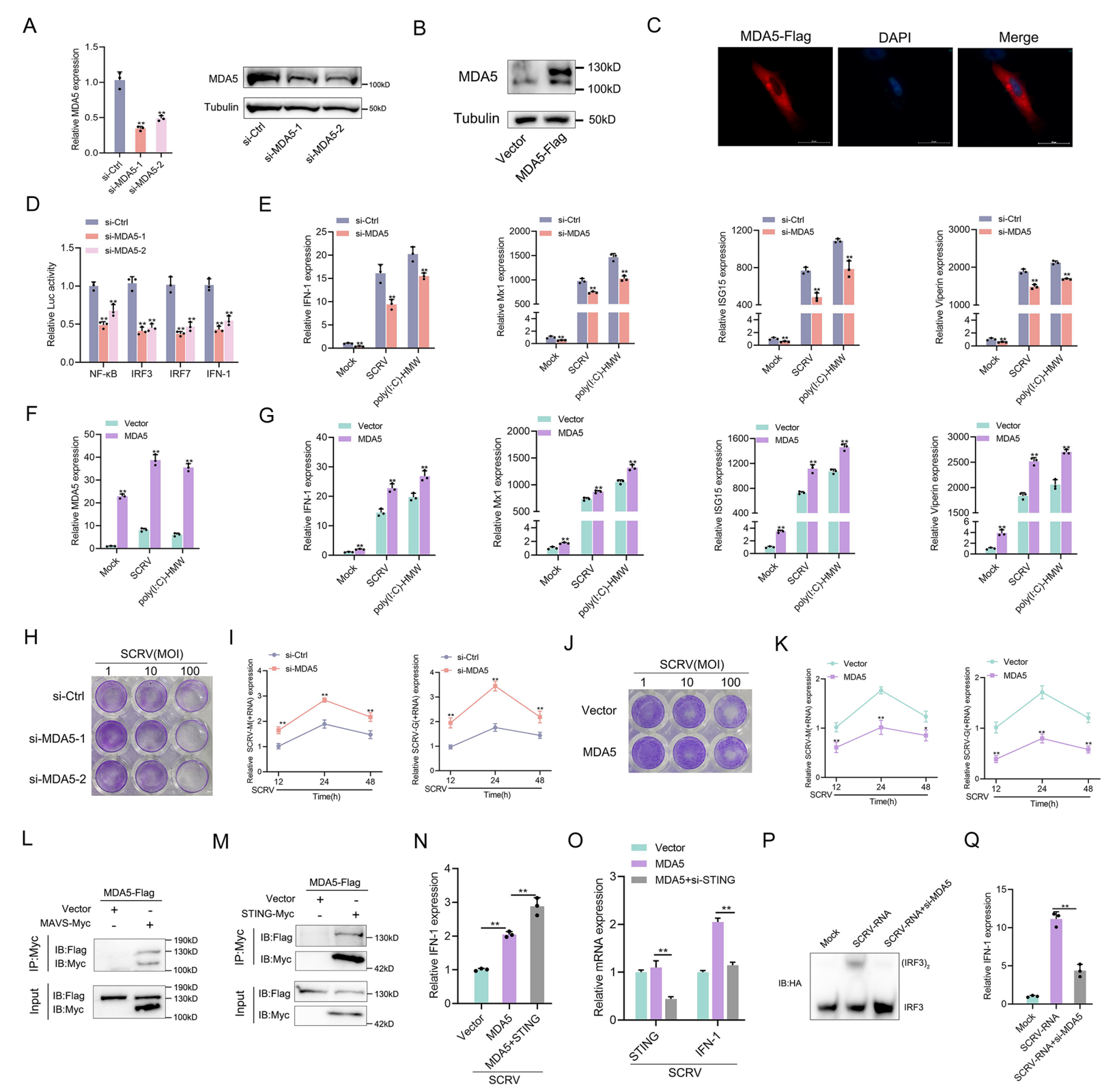
A
Relative MDA5 expression
si-Ctrl
si-MDA5-1
si-MDA5-2
MDA5
Tubulin
100kD
50kD
B
MDA5
Tubulin
130kD
100kD
50kD
Vector
MDA5-Flag
C
MDA5-Flag
DAPI
Merge
D
Relative Luc activity
NF-κB
IRF3
IRF7
IFN-1
E
Relative IFN-1 expression
Relative Mx1 expression
Relative ISG15 expression
Relative Viperin expression
Mock
SCRV
poly(I:C)-HMW
F
Relative MDA5 expression
G
H
SCRV(MOI)
1
10
100
I
Relative SCRV-M(+RNA) expression
Relative SCRV-G(+RNA) expression
Time(h)
J
K
L
MDA5-Flag
MAVS-Myc
IP:Myc
IB:Flag
IB:Myc
Input
M
STING-Myc
N
O
MDA5+si-STING
STING
IFN-1
P
IB:HA
(IRF3)2
IRF3
Q

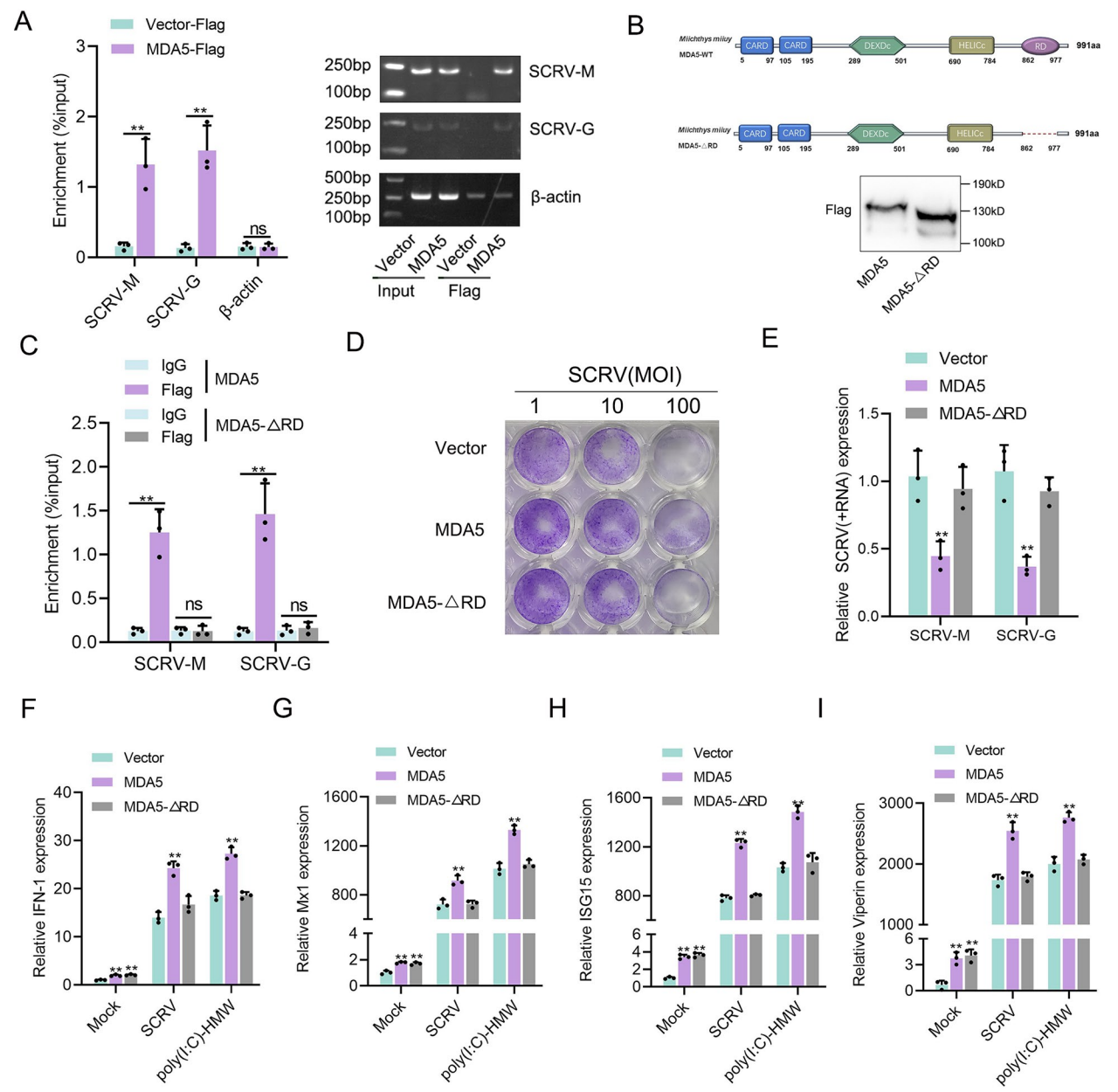
A
Vector-Flag
MDA5-Flag
Enrichment (%input)
SCRV-M
SCRV-G
β-actin
ns
250bp
100bp
500bp
Vector
MDA5
Input
Flag
B
Miichthys miiuy
MDA5-WT
CARD
DEXDc
HELICc
RD
991aa
MDA5-△RD
Flag
190kD
130kD
100kD
C
IgG
Flag
MDA5
MDA5-△RD
D
SCRV(MOI)
1
10
100
Vector
MDA5
MDA5-△RD
E
Relative SCRV(+RNA) expression
F
Relative IFN-1 expression
Mock
SCRV
poly(I:C)-HMW
G
Relative Mx1 expression
H
Relative ISG15 expression
I
Relative Viperin expression

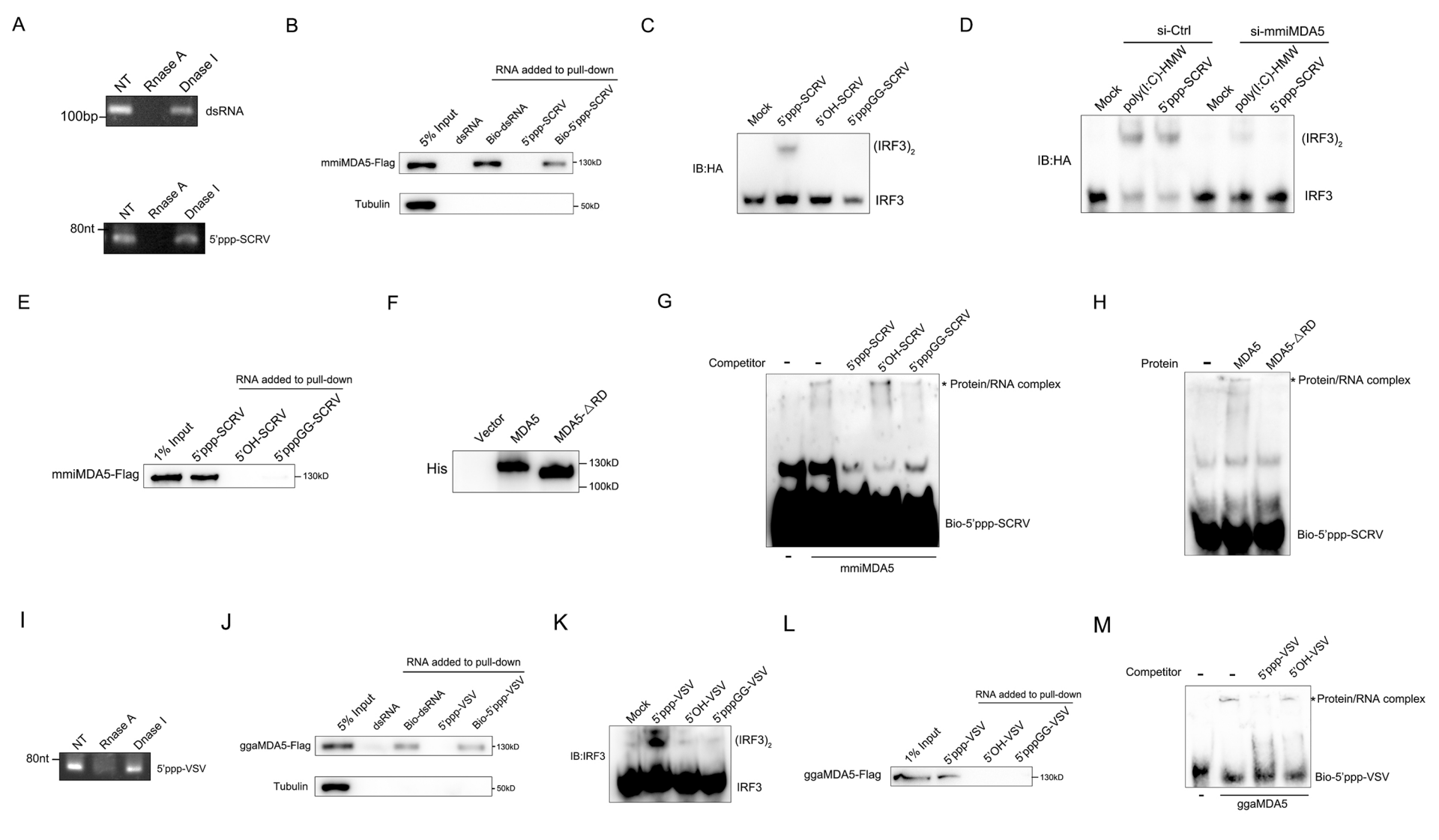
A
NT
Rnase A
Dnase I
100bp
dsRNA
NT
Rnase A
Dnase I
80nt
5'ppp-SCRV
B
RNA added to pull-down
5% Input
dsRNA
Bio-dsRNA
5'ppp-SCRV
Bio-5'ppp-SCRV
mmiMDA5-Flag
130kD
Tubulin
50kD
C
Mock
5'ppp-SCRV
5'OH-SCRV
5'pppGG-SCRV
IB:HA
(IRF3)2
IRF3
D
si-Ctrl
si-mmiMDA5
Mock
poly(I:C)-HMW
5'ppp-SCRV
Mock
poly(I:C)-HMW
5'ppp-SCRV
IB:HA
(IRF3)2
IRF3
E
RNA added to pull-down
1% Input
5'ppp-SCRV
5'OH-SCRV
5'pppGG-SCRV
mmiMDA5-Flag
130kD
F
Vector
MDA5
MDA5-ΔRD
His
130kD
100kD
G
Competitor
-
-
5'ppp-SCRV
5'OH-SCRV
5'pppGG-SCRV
* Protein/RNA complex
Bio-5'ppp-SCRV
-
mmiMDA5
H
Protein
-
MDA5
MDA5-ΔRD
* Protein/RNA complex
Bio-5'ppp-SCRV
I
NT
Rnase A
Dnase I
80nt
5'ppp-VSV
J
RNA added to pull-down
5% Input
dsRNA
Bio-dsRNA
5'ppp-VSV
Bio-5'ppp-VSV
ggaMDA5-Flag
130kD
Tubulin
50kD
K
Mock
5'ppp-VSV
5'OH-VSV
5'pppGG-VSV
IB:IRF3
(IRF3)2
IRF3
L
RNA added to pull-down
1% Input
5'ppp-VSV
5'OH-VSV
5'pppGG-VSV
ggaMDA5-Flag
130kD
M
Competitor
-
-
5'ppp-VSV
5'OH-VSV
*Protein/RNA complex
Bio-5'ppp-VSV
-
ggaMDA5

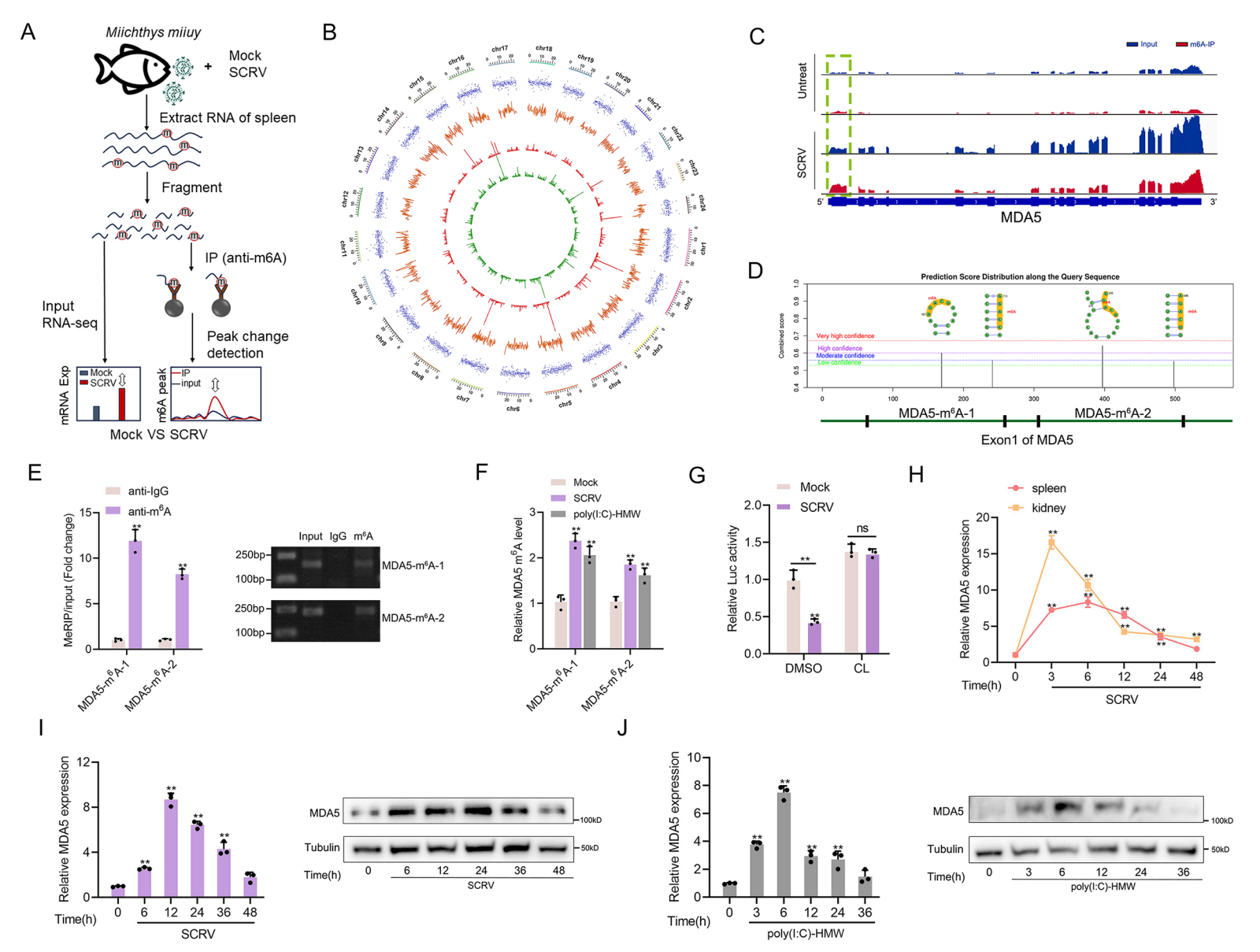
A
Miichthys miiuy
Mock
SCRV
Extract RNA of spleen
Fragment
IP (anti-m6A)
Input
RNA-seq
Peak change
detection
mRNA Exp
Mock
SCRV
m6A peak
IP
input
Mock VS SCRV
B
C
Input
m6A-IP
Untreat
SCRV
5'
3'
MDA5
D
Prediction Score Distribution along the Query Sequence
Combined score
Very high confidence
High confidence
Moderate confidence
Low confidence
MDA5-m6A-1
MDA5-m6A-2
Exon1 of MDA5
E
anti-IgG
anti-m6A
MeRIP/Input (Fold change)
MDA5-m6A-1
MDA5-m6A-2
Input
IgG
m6A
250bp
100bp
F
Mock
SCRV
poly(I:C)-HMW
Relative MDA5 m6A level
G
Mock
SCRV
Relative Luc activity
DMSO
CL
ns
H
spleen
kidney
Relative MDA5 expression
Time(h)
SCRV
I
Relative MDA5 expression
Time(h)
SCRV
MDA5
Tubulin
100kD
50kD
J
Relative MDA5 expression
Time(h)
poly(I:C)-HMW
MDA5
Tubulin
100kD
50kD

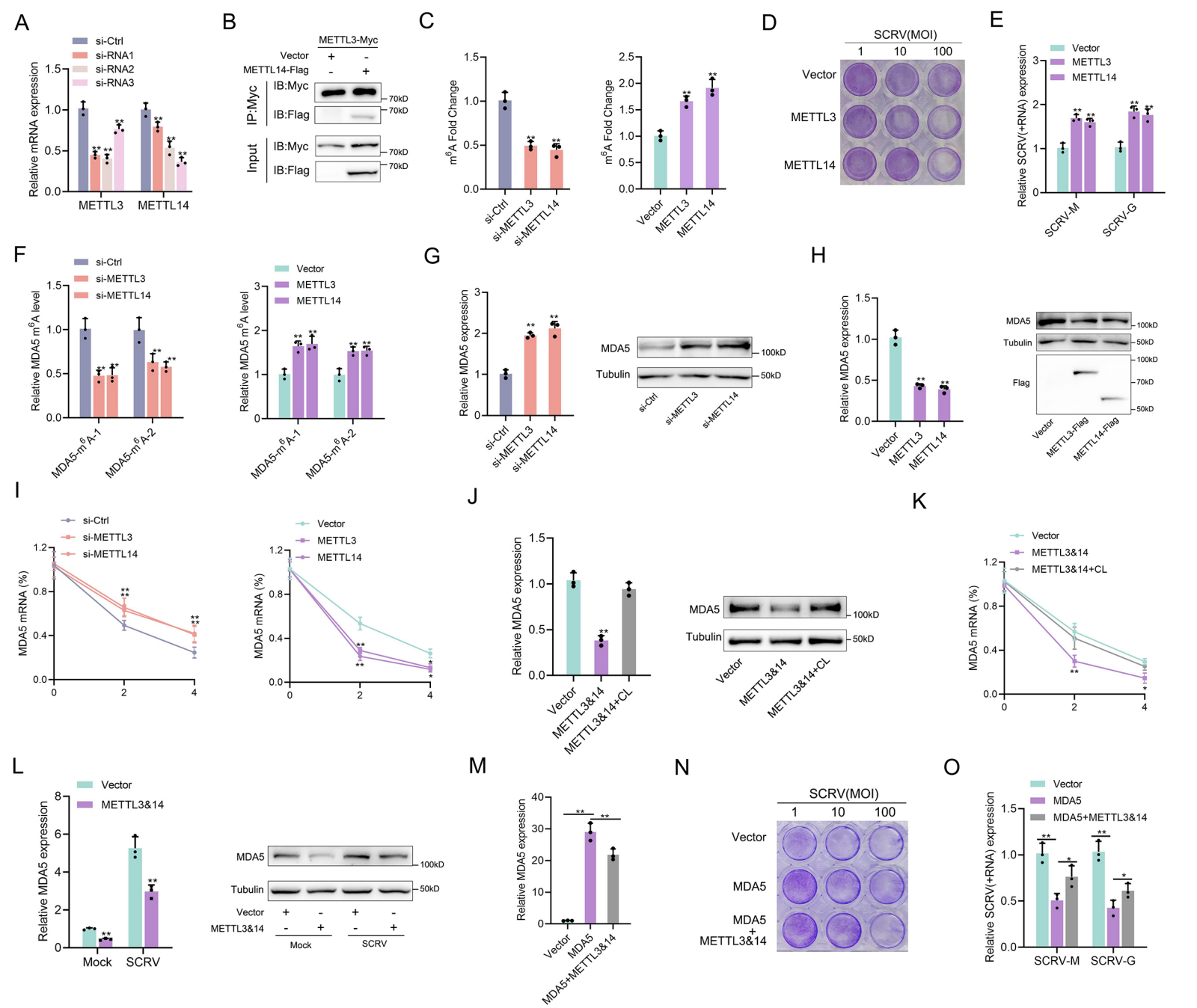
A
si-Ctrl
si-RNA1
si-RNA2
si-RNA3
Relative mRNA expression
METTL3
METTL14
B
METTL3-Myc
Vector
METTL14-Flag
IP:Myc
IB:Myc
IB:Flag
Input
IB:Myc
IB:Flag
70kD
C
m6A Fold Change
si-Ctrl
si-METTL3
si-METTL14
Vector
METTL3
METTL14
D
SCRV(MOI)
1
10
100
Vector
METTL3
METTL14
E
Vector
METTL3
METTL14
Relative SCRV(+RNA) expression
SCRV-M
SCRV-G
F
si-Ctrl
si-METTL3
si-METTL14
Relative MDA5 m6A level
MDA5-m6A-1
MDA5-m6A-2
Vector
METTL3
METTL14
G
Relative MDA5 expression
si-Ctrl
si-METTL3
si-METTL14
MDA5
Tubulin
100kD
50kD
H
Relative MDA5 expression
Vector
METTL3
METTL14
MDA5
Tubulin
Flag
100kD
70kD
50kD
Vector
METTL3-Flag
METTL14-Flag
I
si-Ctrl
si-METTL3
si-METTL14
MDA5 mRNA (%)
Vector
METTL3
METTL14
J
Relative MDA5 expression
Vector
METTL3&14
METTL3&14+CL
MDA5
Tubulin
100kD
50kD
K
Vector
METTL3&14
METTL3&14+CL
MDA5 mRNA (%)
L
Vector
METTL3&14
Relative MDA5 expression
Mock
SCRV
MDA5
Tubulin
100kD
50kD
Vector
METTL3&14
Mock
SCRV
M
Relative MDA5 expression
Vector
MDA5
MDA5+METTL3&14
N
SCRV(MOI)
1
10
100
Vector
MDA5
MDA5 + METTL3&14
O
Vector
MDA5
MDA5+METTL3&14
Relative SCRV(+RNA) expression
SCRV-M
SCRV-G

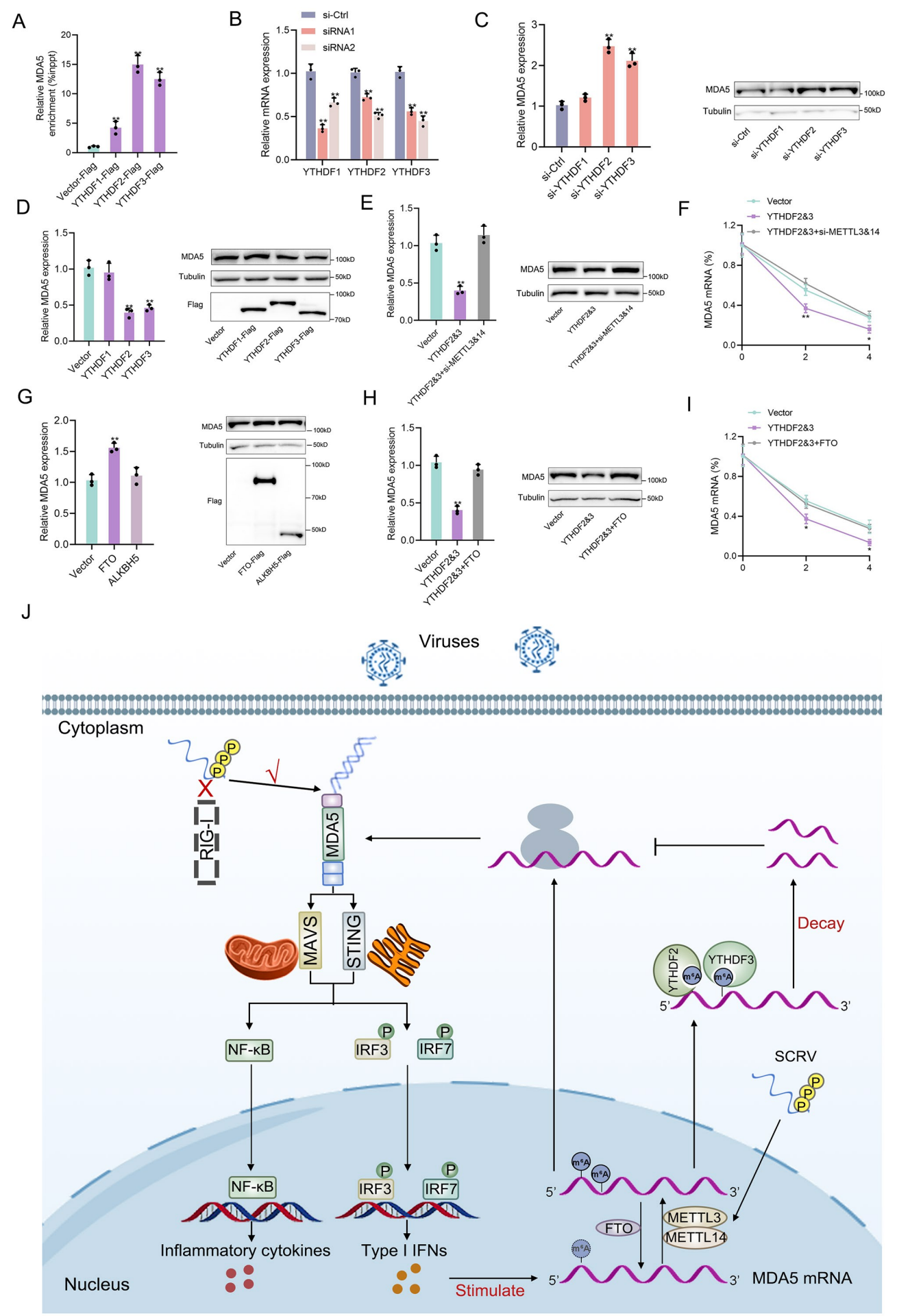
A
Relative MDA5 enrichment (%input)
Vector-Flag
YTHDF1-Flag
YTHDF2-Flag
YTHDF3-Flag
B
si-Ctrl
siRNA1
siRNA2
Relative mRNA expression
YTHDF1
YTHDF2
YTHDF3
C
Relative MDA5 expression
si-Ctrl
si-YTHDF1
si-YTHDF2
si-YTHDF3
MDA5
Tubulin
100kD
50kD
D
Relative MDA5 expression
Vector
YTHDF1
YTHDF2
YTHDF3
Flag
70kD
E
YTHDF2&3
YTHDF2&3+si-METTL3&14
F
Vector
YTHDF2&3
YTHDF2&3+si-METTL3&14
MDA5 mRNA (%)
G
FTO
ALKBH5
FTO-Flag
ALKBH5-Flag
H
YTHDF2&3+FTO
I
YTHDF2&3+FTO
J
Viruses
Cytoplasm
RIG-I
MDA5
MAVS
STING
NF-κB
IRF3
IRF7
Inflammatory cytokines
Type I IFNs
Nucleus
Stimulate
Decay
YTHDF2
YTHDF3
m6A
5'
3'
SCRV
FTO
METTL3
METTL14
MDA5 mRNA